Nanoscale

A Solid-State Colorimetric Fluorescent Pb2+-Sensing Scheme: Mechanically-Driven CsPbBr3 Nanocrystallization in Glass

Journal:	*Nanoscale*
Manuscript ID	NR-ART-03-2020-001818.R1
Article Type:	Paper
Date Submitted by the Author:	26-Mar-2020

Complete List of Authors:	Zhang, Liqiang; Fujian Institute of Research on the Structure of Matter Lin, Hang; Fujian Institute of Research on the Structure of Matter, Wang, Congyong; Fujian Institute of Research on the Structure of Matter, Chinese Academy of Sci Liu, Wei-Ren; Chung Yuan Christian University, Department of Chemical Engineering Li, Shuxing; Xiamen Univ, Cheng, Yao; Fujian Institute of Research on the Structure of Matter, Chinese Academy of Sci, Xu, Ju; Fujian Institute of Research on the Structure of Matter, Chinese Academy of Sci, Gao, Hang; Fujian Institute of Research on the Structure of Matter, Chinese Academy of Sci Li, Kang; University of South Wales Copner, Nigel; University of South Wales Chen, Xueyuan; Fujian Institute of Research on the Structure of Matter, Chin Acad Sci, Wang, Yuansheng; Fujian Institute of Research on the Structure of Matter, Chinese Academy of Sci,

Nanoscale

Guidelines for Referees

Thank you very much for agreeing to review this manuscript for *Nanoscale*.

Nanoscale is a high impact international journal, publishing high quality research across nanoscience and nanotechnology. It publishes a full mix of research articles on experimental and theoretical work, including reviews, communications and full papers.

Nanoscale Associate Editors stress very high standards for acceptance in the journal. Articles must report extremely novel, very high quality, reproducible new work of broad general interest.

Nanoscale's Impact Factor is **6.970** (2018 Journal Citation Reports®)

The following manuscript has been submitted for consideration as a

PAPER

For acceptance, papers must report original scientific work that has not been published previously. Full papers do not have a page limit and should be appropriate in length for scientific content.

When preparing your report, please:

- Focus on the **originality**, **importance**, **impact** and **reproducibility** of the science.
- Refer to the **journal scope and expectations**.
- **State clearly** whether you think the article should be accepted or rejected and give detailed comments (with references) both to help the Editor to make a decision on the paper and the authors to improve it
- **Inform the Editor** if there is a conflict of interest, a significant part of the work you cannot review with confidence or if parts of the work have previously been published.
- **Provide your report rapidly** or inform the Editor if you are unable to do so.

Best regards,

Professor Chunli Bai
Editor-in-Chief, *Nanoscale*

Professor Dirk Guldi
Editor-in-Chief, *Nanoscale*

Dr Michaela Muehlberg
Managing Editor, *Nanoscale*

Contact us

Please visit our reviewer hub for further details of our processes, policies and reviewer responsibilities as well as guidance on how to review, or click the links below.

What to do when you review

Reviewer responsibilities

Process & policies

Letter to Referees

Dear Editor/Referees,

Please find the enclosed manuscript entitled "A Solid-State Colorimetric Fluorescent Pb^{2+}-Sensing Scheme: Mechanically-Drivien $CsPbBr_3$ Nanocrystallizaiton in Glass" by Liqiang Zhang, Hang Lin,* Congyong Wang, Wei-Ren Liu, Shuxing Li, Yao Cheng, Ju Xu, Hang Gao, Kang Li, Nigel Copner, Xueyuan Chen, Yuansheng Wang*, to be considered for publication in *Nanoscale*.

The motive of this work is developing a novel solid-state fluorescent Pb^{2+}-sensing method to detect highly toxic Pb^{2+} in target analyte. In this work, we developed a new kind of Pb^{2+} responsive glass powder, which can produce $CsPbBr_3$ nanocrystals on glass surface upon grinding with Pb^{2+} sources, based on a mechanically-driven glass crystallization mechanism. Utilizing Pb^{2+}-dependent green emission of $CsPbBr_3$ as indicator signal and Pb^{2+}-independent red emission of Eu^{3+} doped in glass as reference signal, it is demonstrated an effective colorimetric fluorescent Pb^{2+}-sensing scheme able to visually perceive Pb^{2+} by naked eyes, and quantitatively/semi-quantitatively detect Pb^{2+} by spectrometer and smartphone.

The work described has not been submitted elsewhere for publication, in whole or in part, and all the authors listed have approved the manuscript that is enclosed.

Sincerely yours,

Yuansheng Wang

Fujian Institute of Research on the Structure of Matter, CAS, China

Tel/Fax: 86-591-63179438

E-Mail: yswang@fjirsm.ac.cn

Response to Reviewer's Comments

Dear Professor Sun and Reviewers,

Thanks for the comments on my manuscript "A Solid-State Colorimetric Fluorescent Pb^{2+}-Sensing Scheme: Mechanically-Driven $CsPbBr_3$ Nanocrystallization in Glass" (ID: NR-ART-03-2020-001818). We appreciate and accept the modification suggestions and have revised the manuscript accordingly. The revised parts are shown in red font. The detailed responses to the reviewer's comments are presented as follows:

Reviewer 1

In this manuscript, it was demonstrated a brand-new solid-state colorimetric fluorescent Pb^{2+}-sensing scheme, showing merits of low cost, high selectivity, and on-site real-time detection. Pb^{2+}-sensing mechanism follows the phase transformation of Cs-Pb-Br from amorphous to crystalline driven by mechanical force. The Pb^{2+}-concentration dependent color variation with green emission of $CsPbBr_3$ as indicator signal and red emission of Eu^{3+} as reference signal enables intuitive Pb^{2+}-sensing by naked eyes and quantitatively determined by spectrometer and smartphone. In my opinion, these results are quite interesting and benefit the development of portable and quick Pb^{2+} analysis method for daily life purpose. Therefore, I recommend its publication in Nanoscale after incorporating some minor revisions:

Comment 1:

The author took lead acetate as Pb^{2+}-source to carry out experiments. How about the results of tests for other lead-containing substances?

Response 1:

We had performed the experiments by using the other lead-containing substances, for example, PbF_2, PbO, $PbBr_2$ *etc.* The studied Eu-BZCKCN glass powders were also responsive to these lead-containing substances by producing $CsPbBr_3$

naonocrystals on glass surface upon grinding. This statement has been added in the revised manuscript (see Page 7).

Comment 2:

In Page 6, it is stated this new method can also be applied to liquid-phase detection? Please provide more discussions on this point.

Response 2:

One can dissolve Pb^{2+} salt in water and then dilute into certain concentration. For Pb^{2+}-sensing experiment, a small amount of solution is dripped into Eu-BZCKCN glass powder for reaction upon grinding. This statement has been added in the revised manuscript (see Page 5).

Reviewer 2

In this work, it is proposed a new kind of Pb^{2+}-responsive material, the Eu-BZCKCN glass powder, which can react with Pb^{2+}-contained substance upon grinding to precipitate the $CsPbBr_3$ perovskite QDs on glass surface. Based on this, it is developed a new solid-state fluorescent Pb^{2+}-sensing scheme, enabling quantitative Pb^{2+} detection via spectrophotometeror semi-quantitative Pb^{2+} detection via smartphone. In my opinion, these results can appeal broad interests among researchers in the related fields. The manuscript is well organized and written, and the discussions are in-depth and persuasive as well.Therefore, I am supportive of its publicationin Nanoscaleafter the authors addressing appropriately the following issues:

Comment 1:

Why choosing the red emission of Eu^{3+} as reference signal? Please give some explanations.

Response 1:

The reasons are as follows: 1) Both of Eu^{3+} and $CsPbBr_3$ nanocrystals can be efficiently excited by UV light, which is a prerequisite for colorimetric fluorescence detection. 2) There is a good signal discriminability for free of spectral overlap between the red emission of Eu^{3+} and the green emission of $CsPbBr_3$ nanocrystals,

which is favorable to distinguish Pb^{2+} concentration dependent color variation, either for naked eyes observation or for spectroscopic detection.

Comment 2:

What is the difference between the present stress-induced glass crystallization method with the previously-reported mechanochemical synthesis method to produce $CsPbBr_3$ (J. Phys. Chem. Lett. 2017, 8, 1610; Chem. Eur. J. 2018, 24, 1811; and J. Mater. Chem. C, 2019,7, 11406)? Please add some discussions/comments.

Response 2:

For the previously-reported mechanochemical synthesis method, the raw materials with crystalline nature, such as, CsBr and $PbBr_2$ are directly blended and then milled to produce $CsPbBr_3$ nanocrystals. For the present stress-induced glass crystallization method, a phase transformation from amorphous to crystalline occurs upon grinding. Therefore, a much more complicated physical/chemical process is involved in the latter case.

Comment 3:

In the inset of Fig.2d, the font size of the labeled Miller indices is too small. I suggest combining Fig.5b and Fig. 5c into one image, as that of Fig.4b.

Response 3:

As suggested, we have enlarged the labeled Miller indices in the inset of Fig.2d. We have also combined Fig.5b and Fig.5c into one image in the revised manuscript.

Comment 4:

There are some grammar mistakes in the text: such as, In Page 12, “crystalinity” should be corrected as “crystallinity”. In Page 15, “smarphone”should be corrected as “smartphone”. Please also check the references to ensure their uniform style.

Response 4:

Thanks for your kind reminder. We have carefully examined the whole manuscript and made several corrections for the grammar mistakes. We have also

checked the References Section to ensure their uniform style.

Sincerely yours,

Yuansheng Wang,

Fujian Institute of Research on the Structure of Matter, CAS, Fuzhou, China

A Solid-State Colorimetric Fluorescent Pb^{2+}-Sensing Scheme: Mechanically-Driven $CsPbBr_3$ Nanocrystallization in Glass

Liqiang Zhang,[a] Hang Lin,[,a] Congyong Wang,[a] Wei-Ren Liu,[b] Shuxing Li,[c] Yao Cheng,[a] Ju Xu,[a] Hang Gao,[a] Kang Li,[d,e] Nigel Copner,[d,e] Xueyuan Chen,[a] Yuansheng Wang[*,a]*

[a] Key Laboratory of Optoelectronic Materials Chemistry and Physics, Key Laboratory of Design and Assembly of Functional Nanostructures, Fujian Institute of Research on the Structure of Matter, Chinese Academy of Sciences, Fuzhou, Fujian 350002, China;
[b] Department of Chemical Engineering, R&D Center for Membrane Technology, Research Center for Circular Economy, Chung Yuan Christian University, Chung Li, Taiwan;
[c] College of Materials, Xiamen University, Xiamen, Fujian 361005, China;
[d] Wireless & Optoelectronics Research & Innovation Centre, Faculty of Computing, Engineering & Science, University of South Wales, Wales, CF37 1DL, UK;
[e] Foshan Huikang Optoelectronics Ltd., Foshan 528000, China;

[*] Corresponding Authors. E-mail: lingh@fjirsm.ac.cn; yswang@fjirsm.ac.cn

E-mail: lingh@fjirsm.ac.cn; Tel/Fax: +86-591-63179423
E-mail: yswang@fjirsm.ac.cn; Tel/Fax: +86-591-63179438

Abstract:

Highly toxic Pb^{2+} poses a great threat to the health of human beings and ecosystem, urgently calling for efficient Pb^{2+} detection method. Herein, it is demonstrated a brand-new solid-state fluorescent Pb^{2+}-sensing scheme based on a kind of Pb^{2+}-responsive borate glass powder that is able to precipitate $CsPbBr_3$ nanocrystals on glass surface upon grinding with Pb^{2+} sources, following a mechanically-driven glass crystallization mechanism. Pb^{2+} sensing is achieved by using Pb^{2+} concentration dependent green emission of $CsPbBr_3$ as indicator signal and that independent red emission of Eu^{3+} as reference signal. Under UV light irradiation, the obvious emissive color variation from red to green as Pb^{2+} concentration varies enables the intuitive Pb^{2+}-sensing by naked eyes. With the aids of spectrometer and smartphone, Pb^{2+} concentration can be quantitatively determined with the detection limit as low as ~70 ppm and ~400 ppm, respectively. The semi-quantitative Pb^{2+} detection is also possible by comparing the emissive color with the calibrated color card. Hopefully, the proposed solid-state fluorescent Pb^{2+}-sensing strategy with high selectivity can be used for portable and quick Pb^{2+} analysis in daily life.

Keywords: Pb^{2+} detection, fluorescent sensing, perovskite nanocrystals, glass crystallization, Eu^{3+}

1. Introduction

Industrial activities have brought not only tremendous wealth for human being, but unfortunately the serious environmental problems, such as heavy metal ion pollution, greenhouse gas emission, plastic abuse, and so on. Among these problems, closely relating with human health, the pollution of highly toxic metal (HTM) ions, including Hg^{2+}, Pb^{2+}, Cd^{2+} and Cr^{6+}, has aroused pressing concerns globally, since these HTM ions are non-biodegradable and accumulative in the environment through contaminating soil, water and food.[1-3] Especially, Pb^{2+} greatly threatens the children by inducing irreversible neurological damage and behavioral dysfunctions.[4-5] Pb^{2+} poisoning can also cause serious diseases, *e.g.*, memory loss, anemia, muscle paralysis, neurasthenia, limb pain, and infertility.[6-7] How to detect Pb^{2+}, even at trace level, has been a matter of vital importance for environmental protection and disease prevention.

Conventionally, Pb^{2+} detection requires sophisticated instrument (*e.g.*, the inductively coupled plasma mass spectrometer, ICP-MS) and follows complex operation procedure (sample pretreatment), and therefore, can only be carried out in the lab by a specially trained person. Recently, Pb^{2+} detection based on fluorescent method gains popularity for the merits of low detection limit, fast response time, and technical simplicity.[8-9] Particularly, with the rapid development of smartphones, the fluorescent parameters (intensity and lifetime) can be readily read by the assembled charge-coupled device (CCD) camera of smartphones, bringing about new advantages of on-site real-time detection and no needs of trained personnel.[10-12]

For the fluorescent Pb^{2+}-sensing method, the basic detection principle is always the same, *i.e.*, luminescent change or colorimetric change (when excited) dependent on Pb^{2+} concentration; however, the Pb^{2+}-sensing materials can be greatly varied from organics to inorganics according to their different application directions, and the corresponding underlying Pb^{2+}-sensing mechanisms are also quite different. One typical example is the small molecule based chemosensor, where the complexation of ligand with Pb^{2+} affects

fluorescence properties by restricting the photo-induced electron transfer with fluorophore,[13] improving electron-accepting ability of some specific groups,[14] or changing the structural conformation.[15] The functionalized Au/Ag nanoparticle is the other kind of efficient Pb^{2+} sensor, and in this case, the chelation/aggregation of Au/Ag nanoparticle in the presence of Pb^{2+} mediated by the functional groups on surface results in plasmon coupling and thus visual color change.[16-17] The functionalized quantum dots (QDs), including semiconductor QDs and carbon QDs, are newly emerged Pb^{2+}-sensors with admirable spectral characteristics of broad absorption and adjustable emission,[18-19] whose Pb^{2+}-sensing properties depend on the chelating reagents bonded to QDs: the chelation of Pb^{2+} with complex could quench QDs exciton emission for the inner filter effect [19-20] or enhance it for the inhibition of adverse fluorescence resonant energy transfer.[21-22] Nevertheless, in spite of the satisfied Pb^{2+} detection effectiveness, state-of-the-art fluorescent Pb^{2+} sensors have their disadvantage respectively. For example, the organic sensor is criticized for the poor photostability and photobleaching;[23] the practical application of Au/Ag nanoparticle is hindered by ultrahigh price;[24] and some semiconductor QDs contain highly toxic Cd,[21-22] *etc*. Moreover, all these materials are prepared via liquid-phase route, generating serious concerns of using environment-unfriendly organic solvent, low production rate, and complex preparation procedure. When applying these materials to Pb^{2+}-sensing, some other technical issues arise: 1) the liquid environment is required, and so the target analyte should be dissolved, which is inconvenient for detecting solid samples; 2) the detection accuray is subjected to acidity/alkalinity of solvent; and 3) the possible interference of the other metal ions——the detection selectivity matters.

In the present work, we proposed a new solid-state Pb^{2+}-sensing strategy based on mechanically-driven glass crystallization of $CsPbBr_3$ perovskite nanocrystals (NCs) in a Pb^{2+}-responsive borate glass system. Utilizing Pb^{2+}-dependent green emission of $CsPbBr_3$ as indicator signal and Pb^{2+}-independent red emission of Eu^{3+} as reference signal, it is

demonstrated an effective colorimetric fluorescent Pb^{2+}-sensing scheme able to visually perceive Pb^{2+} by naked eyes, and quantitatively/semi-quantitatively detect Pb^{2+} by spectrometer and mobile smartphone.

2. Experimental

2.1 Synthesis of Pb^{2+}-responsive glass powder:

The Eu^{3+} doped precursor glass (PG) with stoichiometric composition (in mol%) of $50B_2O_3$-10ZnO-10CaO-$5K_2O$-$10Cs_2O$-15NaBr (abbreviated as Eu-BZCKCN glass) was fabricated via a melt-quenching route. The raw materials of H_3BO_3, ZnO, $CaCO_3$, K_2CO_3, Cs_2CO_3, NaBr, and Eu_2O_3 were weighted and mixed thoroughly in an agate mortar and melted in a Al_2O_3 crucible at 950 ℃ for 30 min under an ambient atmosphere. Then, the glass melt was super-cooled down to 150 °C by quickly pouring into a pre-heated copper mold. After holding at 150 °C for 2 h to relinquish inner stress, the bulk PG was obtained, which was further pulverized, ball-milled for 10 h, and screened by a 400-mesh sieve, into the Eu-BZCKCN glass powders.

2.2 Fluorescent Pb^{2+}-sensing:

Fluorescent Pb^{2+} detection was performed by using the Eu-BZCKCN glass powder as Pb^{2+}-sensor, following a facile solid-state route. In a typical procedure, 1 g of the said glass powder was blended with the solid analyte and then fully ground in an agate mortar for 10 min. One can also dissolve Pb^{2+} salt in water, dilute into certain concentration, and then drip a small amount of solution into Eu-BZCKCN glass powder for reaction upon grinding. Under 365 nm UV light excitation, luminescence properties of the ground samples were recorded by the professional spectroscopic measurement or analyzed by the color recognizer software loaded in smartphone after taking photographs by CCD camera. According to the pre-calibrated relationship between Pb^{2+} concentration and luminescence intensity/RGB color information, one can determine the Pb^{2+} concentration in the analyte.

2.3 Characterization:

Differential scanning calorimetry (DSC, Netzsch, STA449F3) was carried out by heating the Eu-BZCKCN glass powder in an air atmosphere (α-Al_2O_3 crucible) at a heating rate of 10 °C/min. Transmission electron microscope (TEM, JEOL, JEM-2010) observation operating at 200 kV and scanning electron microscope (SEM, JEOL, JSM-6700F) observation equipped with an energy dispersive spectrometer (EDS, Oxford INCA) were performed to characterize microstructure of the precipitated perovskite $CsPbBr_3$ NCs on glass surface. Raman spectra (HORIBA, LabRam HR) were measured to study the glass structural variation dependent on glass composition, using a 633 nm laser as the excitation source. The photoluminescence (PL) and photoluminescence excitation (PLE) spectra were measured by a spectrophotometer (Edinburgh Instruments, FS920) equipped with a 450 W xenon lamp as the excitation source and a photomultiplier tube (R943-02, Hamamatsu) as the detector. Confocal images were taken by a confocal laser scanning microscopy system (C2/Ti-E) equipped with a Plan Fluor VC 20x DIC N2 objective lens (NA 0.5) and Andor ixon3 EMCCD camera.

3. Results and discussions

3.1 Mechanically-driven glass crystallization of $CsPbBr_3$

In Figure. 1a and 1b, one can see the prepared Eu-BZCKCN bulk glass and the corresponding glass powder yield red emission under 365 nm UV light irradiation. The steady-state spectroscopic measurements demonstrate the red emission originates from the parity-forbidden 4f↔4f transitions of Eu^{3+}, as presented in Figure. 1c. The much more intensified Eu^{3+}: $^5D_0 \rightarrow {}^7F_2$ electric-dipole transition at 615 nm than the Eu^{3+}: $^5D_0 \rightarrow {}^7F_1$ magnetic-dipole one at 590 nm reveals that, Eu^{3+} ions, possibly acting as glass network modifiers, are located in a noncentrosymmetric environment.[25] In the experiment, Eu^{3+} doping concentration is optimized as 1.5 mol%, beyond which the bulk PG becomes devitrified and therefore the red emission intensity declines. Interestingly, upon grinding the BZCKCN glass powder with Pb^{2+}-source in solid or liquid state, the ground sample yields green light under 365 nm UV light irradiation (Figure. 1d), indicative of the generation of new photo-active

species. Worthy to be mentioned, in the experiment, we chose lead acetate ($(CH_3COO)_2Pb$) as a representative, while the similar phenomena were found when using the other Pb^{2+}-containing substances, such as, PbF_2, PbO, $PbBr_2$ *etc.* The spectral features in PL/PLE spectra and kinetic decay curve of the ground sample (Figure. 1e and 1f) accord well with the excitonic excitation/emission characteristics of perovskite $CsPbBr_3$.[26-29] From the confocal laser scanning microscope analysis on single one Eu-BZCKCN glass particle (Figure. 1g-1i), it is evident that both of the green and red emissions come from glass powder, and so, this is not the case of simple physical mixture of two luminescent species upon grinding; in other words, the newly generated active centers with green emission should be incorporated into glass.

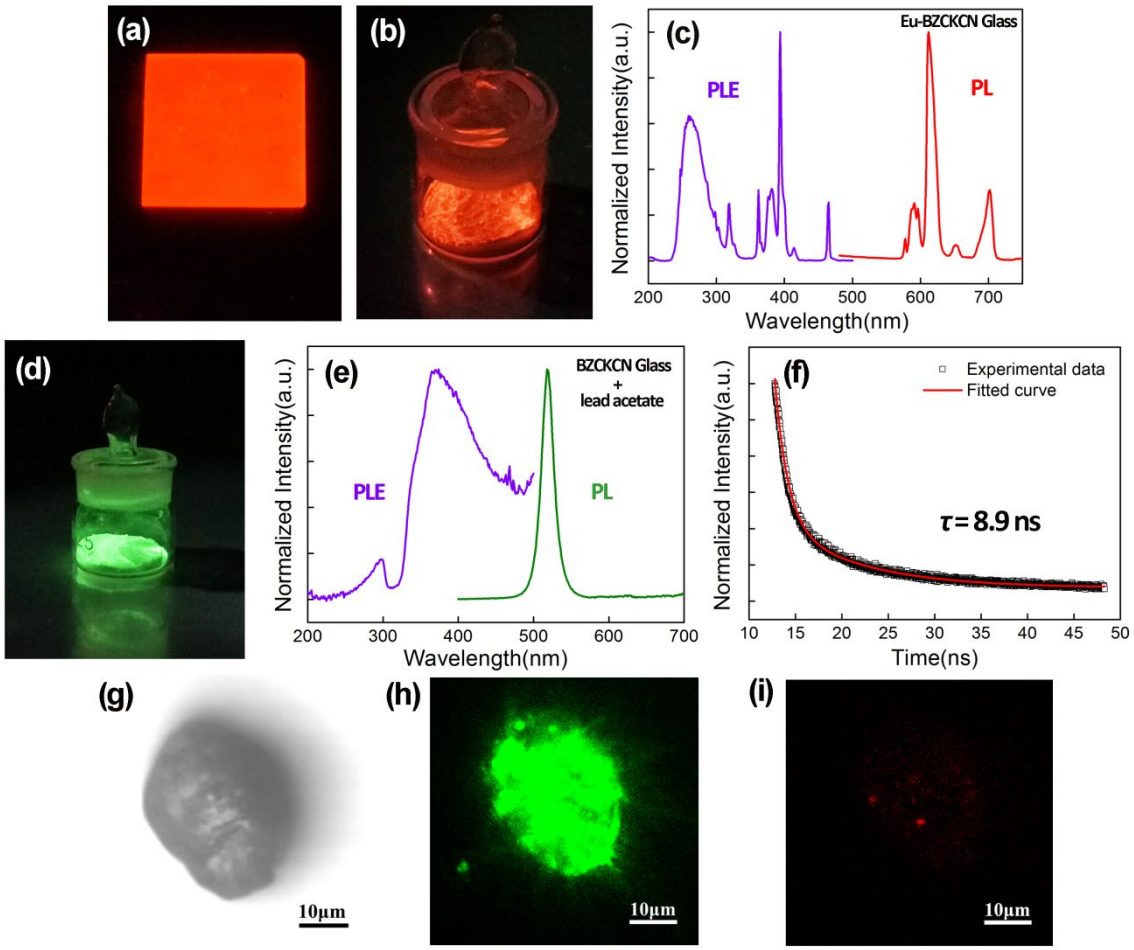

Figure. 1 Luminescent photographs of the prepared (a) Eu-BZCKCN bulk glass and (b) the corresponding glass powder, upon 365 nm UV light irradiation. (c) PL (λ_{ex}=365 nm) and PLE (λ_{em}=615 nm) spectra of the Eu-BZCKCN glass powder. (d) Luminescent photographs after grinding BZCKCN glass powder with lead

acetate, under 365 nm UV light irradiation. (e) PL (λ_{ex}=365 nm) and PLE (λ_{em}=515 nm) spectra and (f) luminescent decay curve (λ_{ex}=365 nm, λ_{em}=515 nm) of the sample after grinding Eu-BZCKCN glass powder with lead acetate. The confocal laser scanning microscope analysis on single one Eu-BZCKCN glass particle excited (g) without and (h, i) with UV laser (λ_{ex}=405 nm); for (h), the detection channel is 525 nm; for (i) the detection channel is785 nm (this is why the red emission looks so weak).

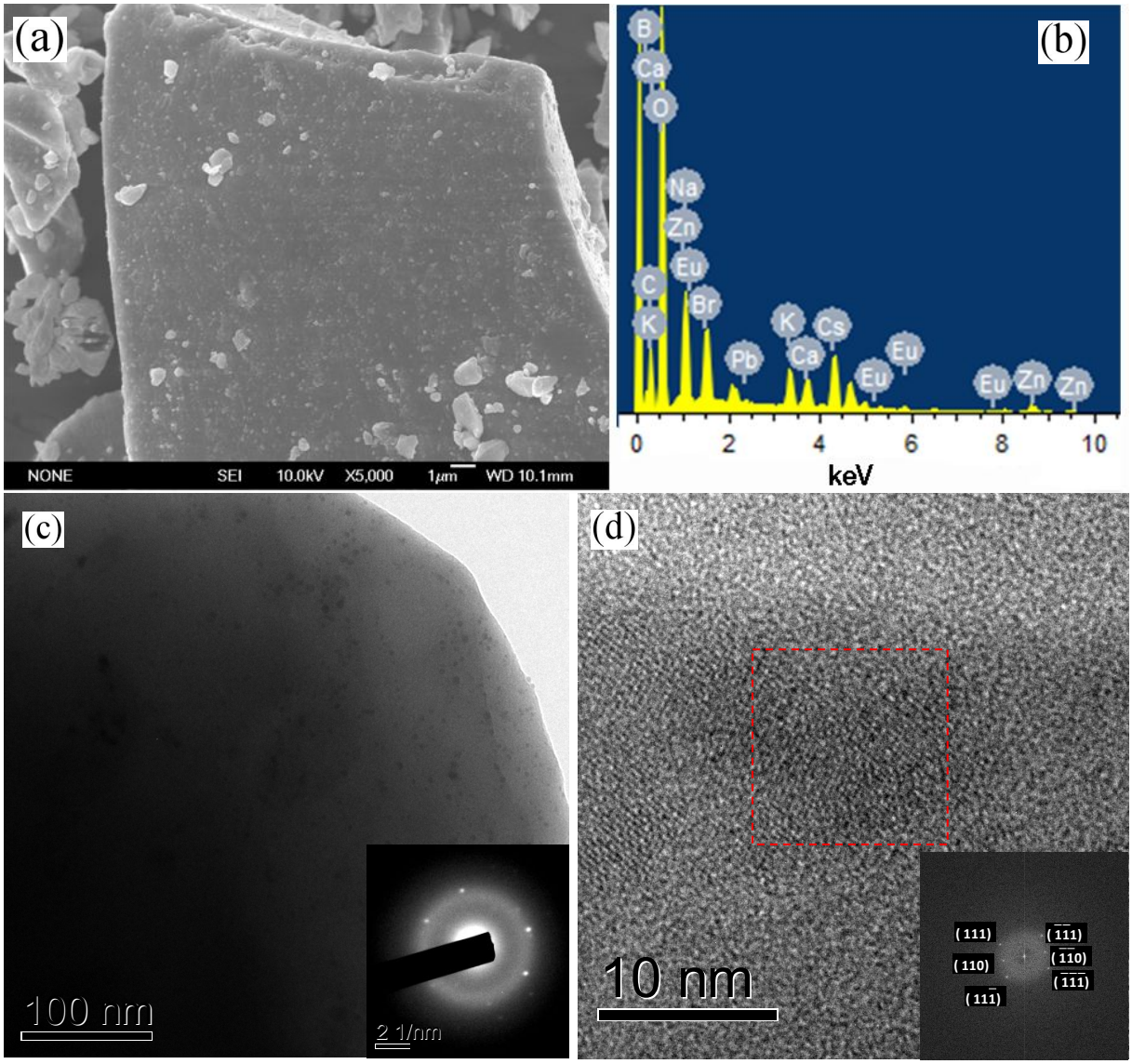

Figure. 2 (a) SEM observation on single one glass particle upon grinding Eu-BZCKCN glass powder with lead acetate, and (b) the corresponding EDS analysis result. (c) Bright-field TEM image of the sample after grinding Eu-BZCKCN glass powder with lead acetate; inset is the corresponding SAED pattern. (d) High-resolution TEM observation on single one $CsPbBr_3$ NC; inset shows the FFT pattern converted from the red dashed square region.

SEM microstructure observation discloses that some tiny particles with size up to several tens or hundreds of nanometers randomly distribute on glass surface (Figure. 2a). EDS analysis on single one glass particle confirms the glass composition of B, Zn, Ca, K, Na, Cs,

Br, O, Eu, and the post-adding Pb is also detected (Figure. 2b). We speculate that Pb^{2+} reacts with Cs^{+} and Br^{-} on glass surface to form $CsPbBr_3$, since the efficient green emitter $CsPbBr_3$ is known to crystallize easily for its ionic nature and ultralow formation energy.[28-31] In the X-ray diffraction (XRD) measurement, $CsPbBr_3$ diffraction peak cannot be discerned, which should be due to its low crystallization fraction (merely crystalizing on glass surface) beyond the detection limit (~5%) of XRD. Fortunately, the existence of $CsPbBr_3$ can be identified in the following TEM observation. The bright-field TEM image in Figure. 2c shows the crystallized $CsPbBr_3$ with size down to several nanometers (in the size range of QDs) that cannot be distinguished by SEM. It is obvious that $CsPbBr_3$ crystalizes in a wide size distribution upon grinding Eu-BZCKCN glass powder with Pb^{2+}-sources. The selected area electronic diffraction (SAED) pattern demonstrates the amorphous halo ring from glass matrix and the polycrystalline diffraction spots from $CsPbBr_3$ (inset of Figure. 2c). In the high-resolution TEM image on single one $CsPbBr_3$ NC (Figure. 2d), one can identify the interplanar spacings of 0.337 nm and 0.425 nm, indexing to (111) and (110) facets, respectively. According to the corresponding two-dimensional fast Fourier transform (FFT) image, the angle between the (111) facet and the (110) one is 36.9°, getting close with the theoretical one of 35.3°. Combining these microstructural characterization results, the precipitation of $CsPbBr_3$ NCs on glass surface is confirmed.

The crystallization of $CsPbBr_3$ NCs on Eu-BZCKCN glass surface should be driven by mechanical force. Such glass crystallization mechanism was firstly demonstrated by our group in a phosphate glass system of P_2O_5-$PbBr_2$-NaBr-Cs_2O-SrO.[32] Therein, it was found the breakage of bonding of glass network provides energy for nucleation and growth of $CsPbBr_3$ NCs, and the effect of shear stress avoids long-range migration of structural units for crystallization.[32] In the studied borate glass system of B_2O_3-ZnO-CaO-K_2O-Cs_2O-NaBr, Pb is excluded in glass composition, but is post-added. We performed some experiments to elucidate the proposed crystallization mechanism. As presented in Figure. 3a, DSC curve of

the Eu-BZCKCN glass shows glass transition temperature (T_g) of ~256 °C. Considering that the structural relaxation of glass to induce rearrangement of structural units should be at least higher than T_g, while reaching such high temperature during grinding seems impossible, the conventional heat-induced glass crystallization mechanism is believed not workable in the present case. It is also noticed that not all the Eu-BZCKCN glasses with varied glass compositions result in $CsPbBr_3$ crystallization on glass surface after grinding with Pb^{2+} source. As an example, for $50B_2O_3$-10ZnO-10CaO-$5K_2O$-(25-x)Cs_2O-xNaBr (in mol%, x = 5, 10, 15, 20), the crystallization takes place only when x>15 mol%. Therefore, it can be concluded that the mechanically-driven $CsPbBr_3$ crystallization is principally determined by the nature of glass. In Figure. 3b, we measured Raman spectra of the Eu-BZCKCN glass by varying the relative content of Cs_2O/NaBr. All the Raman peaks accord well with those vibrations of all kinds of boroxol groups.[33-36] As one can see, the structural variation of glass is rather complex. One most prominent difference in spectral feature for the samples able to precipitate $CsPbBr_3$ to those unable one is the more intensified Raman peaks at ~1250 cm^{-1} and ~1600 cm^{-1}. The peaks at 1250 cm^{-1} and ~1600 cm^{-1} are characteristic vibrations of metaborate chains[33] and metaborate rings,[37] respectively, both of which consist of three non-bridging oxygen (NBO) atoms. The other one prominent difference is the disappeared Raman peak at ~560 cm^{-1} in the samples able to precipitate $CsPbBr_3$. This ~560 cm^{-1} peak could be designated as BO_4^- tetrahedron (O represents bridging oxygen).[33] Evidently, the increase of Na and Br contents depolymerizes the glass network to induce more groups with NBO atoms, and the resultant loose glass structure enables the reaction of Cs^+ and Br^- (both acting as glass network modifiers with weak bonding) with Pb^{2+} on glass surface upon grinding. The mechanically-driven glass crystallization mechanism is schematically illustrated in Figure. 3c.

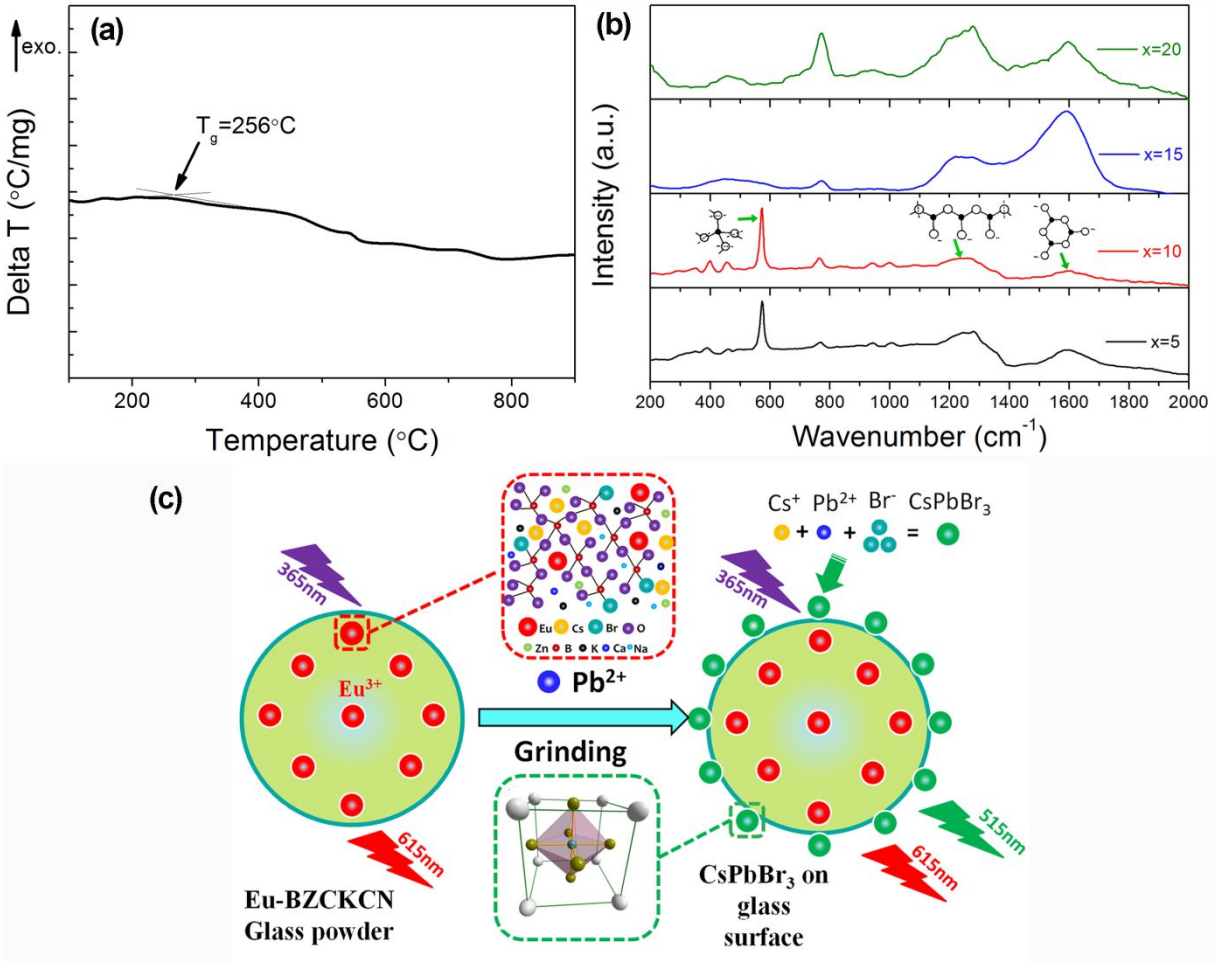

Figure. 3 (a) DSC curve of the Eu-BZCKCN glass powder. (b) Raman spectra of the Eu-BZCKCN glass with varied Cs_2O/NaBr molar ratios in $50B_2O_3$-10ZnO-10CaO-$5K_2O$-(25-x)Cs_2O-xNaBr (in mol%, x = 5, 10, 15, 20). (c) Schematic illustration of the mechanically-driven glass crystallization mechanism.

3.2 Quantitative Pb^{2+} detection via fluorescence spectrophotometer

As stated above, Eu-BZCKCN glass powder yields two-color emission after grinding with Pb^{2+} sources due to the generation of $CsPbBr_3$ NCs. We further examined Pb^{2+} concentration dependent PL spectra of the ground samples under the same instrumental setup, as displayed in Figure. 4a, wherein one can simultaneously identify the spectral features of $CsPbBr_3$ and Eu^{3+}. With the increase of Pb^{2+} concentration from 0 ppm to 3500 ppm, PL intensity of $CsPbBr_3$ gradually gets enhanced, while that of Eu^{3+} is almost unchanged; correspondingly, the PL color observed by naked eyes evolves from red to yellow, and then to green (inset of Figure. 4a). This phenomenon is reasonable: $CsPbBr_3$ NCs generate more and

more and/or they grow up accompanied with improved crystallinity, when more Pb^{2+} is supplied; while Eu^{3+} emission is obviously independent of Pb^{2+} concentration since there is no evidence of energy transfer between $CsPbBr_3$ and Eu^{3+}. The slight red-shift of excitonic emission of $CsPbBr_3$ as increasing of Pb^{2+} concentration implies the larger $CsPbBr_3$ NCs precipitate on glass surface. The more symmetric spectral profile at higher Pb^{2+} concentration suggests the particle size of $CsPbBr_3$ becomes more even. Utilizing the integrated PL intensity of $CsPbBr_3$ as indicator signal ($I_{CsPbBr3}$) and that of Eu^{3+} (I_{Eu3+}) as reference signal, a self-calibrated colorimetric Pb^{2+}-sensing scheme is demonstrated (Figure. 4b). It is found a good linearity between Pb^{2+} concentration and $I_{CsPbBr3}/I_{Eu3+}$ in the range of 0-2500 ppm, following the equation of y=0.00105x+0.5764 (Residual factor, R^2=0.995). Beyond 2500 ppm, the slope decreases, probably caused by the exhaustion of Cs^+/Br^- on glass surface. According to the equation of

$$LOD = 3\sigma / K \quad (1),$$

where LOD is the limit of detection, σ the standard deviation of blank signal, and K the slope of the fitted straight line, LOD of Pb^{2+} detection based on this solid-state fluorescent method is determined as ~70 ppm. This value is inferior to that reported in the liquid-phase fluorescent method (able to reach ppb level[24]). Despite the proposed solid-state fluorescent method is not most effective for fluorescent Pb^{2+} sensing, it is cost-effective and facile, does not bring secondary pollution to environment, and most importantly, is suitable to detect Pb^{2+} in solid form. One can expect it plays a role in detecting Pb^{2+} for solid waste, children's' toy, and so on.

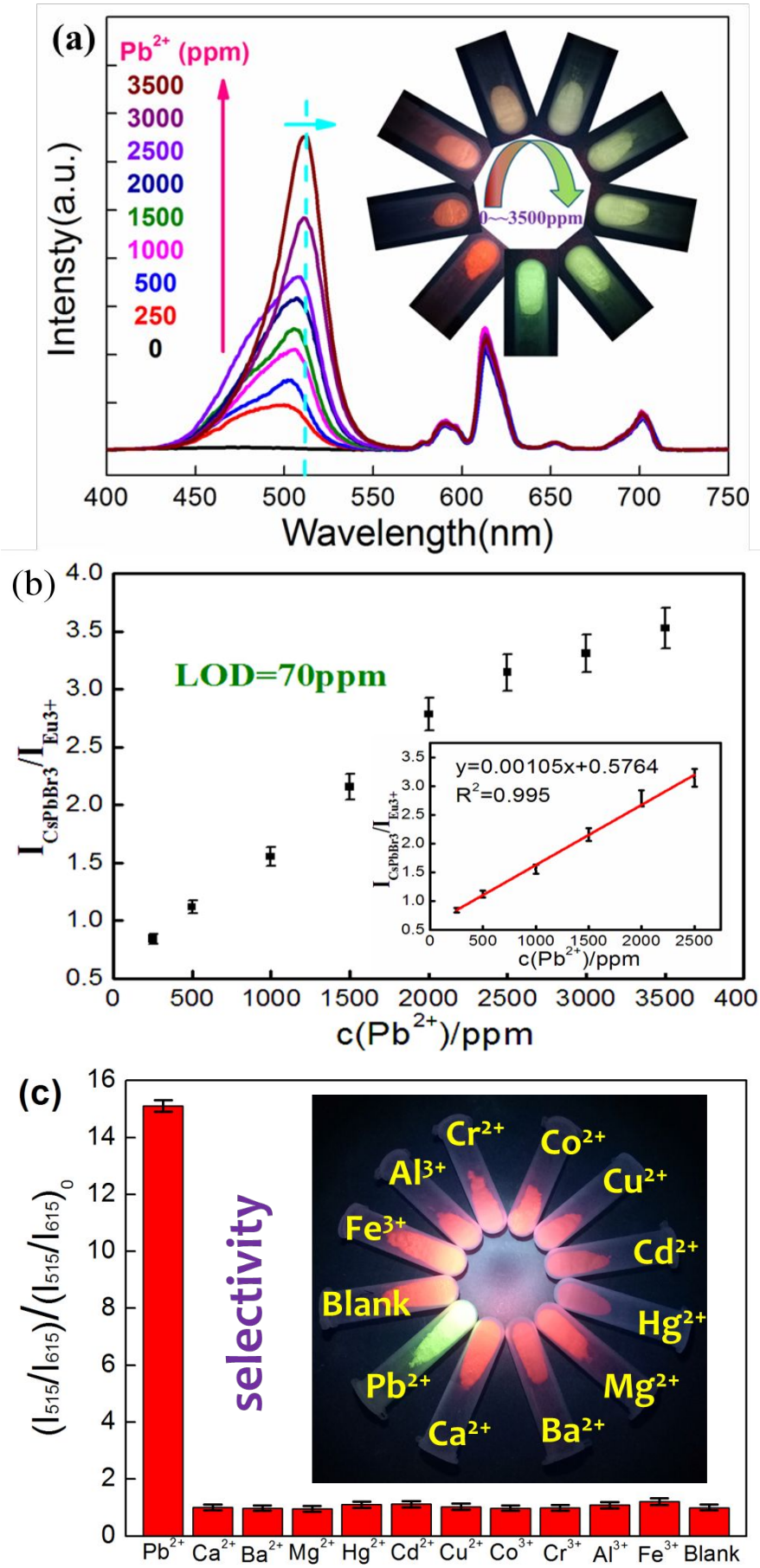
(a)
Pb2+ (ppm)
3500
3000
2500
2000
1500
1000
500
250
0
Intensty(a.u.)
0~~3500ppm
400 450 500 550 600 650 700 750
Wavelength(nm)
(b)
LOD=70ppm
y=0.00105x+0.5764
R2=0.995
ICsPbBr3/IEu3+
c(Pb2+)/ppm
(c)
(I515/I615)/(I515/I615)0
selectivity
Cr2+
Co2+
Al3+
Cu2+
Fe3+
Cd2+
Blank
Hg2+
Pb2+
Mg2+
Ca2+
Ba2+
Pb2+ Ca2+ Ba2+ Mg2+ Hg2+ Cd2+ Cu2+ Co3+ Cr3+ Al3+ Fe3+ Blank

Figure. 4 (a) Pb^{2+} concentration (0-3500 ppm) dependent PL spectra of the ground samples upon 365 nm excitation; the inset shows the corresponding luminescent photographs under 365 nm UV lamp. (b) The plot of the dependence of Pb^{2+} concentration versus $I_{CsPbBr3}/I_{Eu3+,}$ inset shows good linear relationship in the region of 0-2500 ppm. (c) The colorimetric response of other HTM ions or common cations in water/soil utilizing the proposed solid-state fluorescent method; inset shows the corresponding luminescent photographs under 365 nm UV light irradiation.

In order to evaluate the selectivity and anti-interference ability of this solid-sate fluorescent method to detect Pb^{2+}, a series of experiments were performed by grinding the Eu-BZCKCN glass powder in the presence of other HTM ions or common cations in water/soil, such as, Ca^{2+}, Ba^{2+},Mg^{2+}, Hg^{2+}, Cd^{2+}, Cu^{2+}, Co^{2+}, Cr^{3+}, Al^{3+}, and Fe^{3+}, and then measured the corresponding PL spectra of the ground samples. As presented in Figure. 4c, their PL characteristics are almost identical with the Eu-BZCKCN glass powder (as the blank sample), and so the influence of these interfering ions is negligible.

3.2 On-site real-time quantitative/semi-quantitative Pb^{2+} detection via smartphone

Nowadays, the software/hardware technologies of smartphone change with each passing day, allowing ever-closer approach between the user and the access to information. Utilizing the integrated CCD camera, the LED source, and the APP software provided by third-party Company, the spectroscopy applications of smartphones, such as, NIR light for food analysis,[38-39] smart QR codes for luminescence thermometry,[40] persistent luminescence for anti-counterfeiting,[41] as well as, fluorescent Pb^{2+}-sensing,[19] has been proposed and demonstrated recently. Herein, we will show the proposed solid-state fluorescent Pb^{2+}-sensing method is also compatible to smartphone technology for portable and quick Pb^{2+} analysis in daily life.

In Figure. 5a, we schematically illustrate the Pb^{2+}-sensing method using smartphone. The luminescent photographs of the ground samples under UV light irradiation are taken by CCD camera. Based on a simple function embedded in color recognizer software downloaded from Oppo APP Market, the color in luminescence photographs can be decomposed into three RGB channels. The obtained RGB values ($I_{green\text{-}channel}/I_{red\text{-}channel}$) correlates with Pb^{2+}

concentration (Figure. 5b). There is a good linear relationship between them in the range of 0-2500 ppm following a function of y=0.000505x+0.414 with R^2=0.986. According to equation (1), LOD of the proposed solid-state fluorescent Pb^{2+}-sensing method with the aid of smartphone is determined as ~400 ppm. A semi-quantitative detection of Pb^{2+} can also be achieved by comparing the Pb^{2+}-dependent luminescent color with the calibrated color card provided by the software.

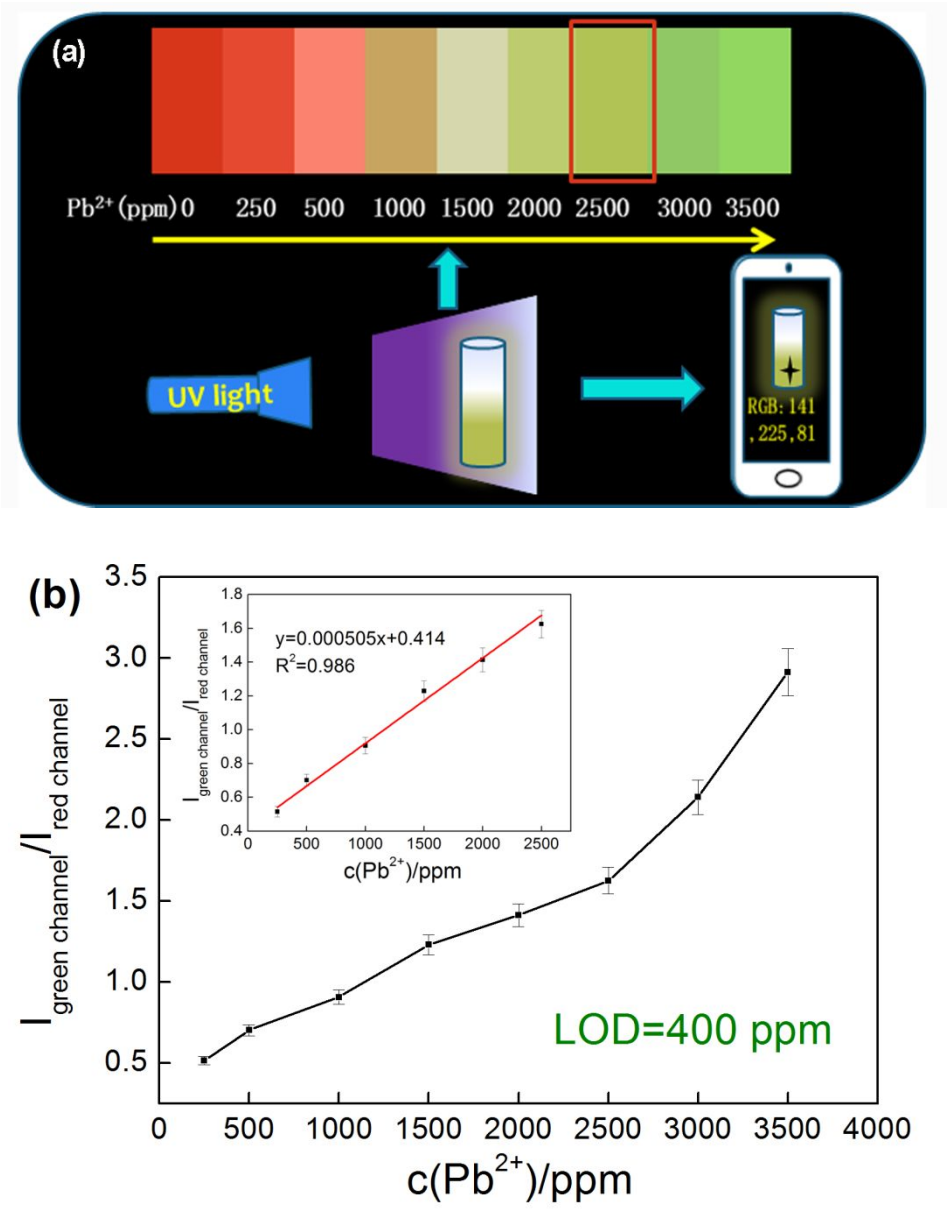

Figure. 5 (a) Schematical illustration of using smartphone to determine Pb^{2+} concentration. (b) The plot of Pb^{2+} concentration dependent color change (green channel/red channel) recognized by smartphone, inset shows good linear relationship in the region of 0-2500 ppm.

4. Conclusion

In summary, it is proposed a novel solid-state fluorescent Pb^{2+}-sensing strategy that partially settles the tough issues of high cost, inconvenience, and environment hazards, *etc.,* in the conventional liquid-phase Pb^{2+}-sensing scheme. Such Pb^{2+}-sensing strategy is achieved by grinding a Pb^{2+}-responsive Eu-BZCKCN glass powder with Pb^{2+} sources. The microstructural characterization demonstrates the precipitation of $CsPbBr_3$ NCs in a wide size distribution on glass surface. According to Raman analyses, the mechanically-driven glass crystallization behavior is closely related with the glass network structure, that is, only those loose glass network with NBO atoms enables the $CsPbBr_3$ crystallizaiton. For colorimetric Pb^{2+} detection, the Pb^{2+} concentration dependent green emission from the crystallized $CsPbBr_3$ can be used as indicator signal, while the Pb^{2+} concentration independent red emission from the doped Eu^{3+} in glass serves as reference signal. Evidently, the color variation makes the visual perception of Pb^{2+} possible. It is also verified the quantitative Pb^{2+} detection via fluorescence spectrophotometer with high selectivity and quantitative/semi-quantitative Pb^{2+} detection via smartphone for portable and quick Pb^{2+} analysis in daily life. The proposed solid-state fluorescent Pb^{2+}-sensing strategy could be realized in the other Cs- and Br- contained glass material system doped with the other active ions.

Author Contribution

H. Lin conceived the solid-state Pb^{2+} sensing scheme. L. Zhang synthesised the Pb^{2+} sensitive glass powder and wrote the first draft. H. Lin helped L. Zhang analyse the experimental results and finish the final manuscript. C. Wang and J. Xu carried out the Pb^{2+} sensing experiment. Y. Cheng helped perform the SEM/TEM measurement. W. Liu and S. Li helped to analyse the Pb^{2+} sensing mechanism. H. Gao and K. Li helped perform the spectroscopy measurements. N. Copner and X. Chen provided constructive suggestions to the data analyses. Y. Wang supervised the project.

Conflicts of interest

There are no conflicts to declare.

Acknowledgements

This work is supported by the National Natural Science Foundation of China (51972303, 11674318, 11974350, 11774346, and 51872288)

References

1 M. F. Philips, A. I. Gopalan, and K. P. Lee, *J. Hazard. Mater.*, 2012, 237, 46-54.

2 X. Qing, Z. Yutong, and G. L. Sheng, *Ecotoxicol. Environ. Saf.*, 2015, 120, 377-385.

3 N. Saha, M. S. Rahman, M. B. Ahmed, J. L. Zhou, H. H. Ngo, and W. Guo, *J. Soil Sci. Environ. Manage.*, 2017, **185**, 70-78.

4 E. S. Claudio, H. A. Goldwin, and J. S. Magyar, *Prog. Inorg. Chem.*, 2003, 51, 1-144.

5 Q. Zhu, L. Liu, Y. Xing, and X. Zhou, *J. Hazard. Mater.*, 2018, **355**, 50-55.

6 Y. Wang, and J. Irudayaraj, *Chem. Commun.*, 2011, 47, 4394-4396.

7 B. Wang, B. Luo, M. Liang, J. Wang, Y. Fang, and L. Zhi, *Nanoscale*, 2011, 3, 5059-5066.

8 T. Sokalski, A. Ceresas, T. Zwickl, and E. Pretsch, *J. Am. Chem. Soc.*, 1997, **119**, 11347-11348.

9 J. Mayer, A. Robert-Moreno, J. Sharpe, and J. Swoger, *Light: Sci. Appl.*, 2018, **7**, 70.

10 X. Chen, Y. Zhou, X. Peng, and J. Yoon, *Chem. Soc. Rev.*, 2010, 39, 2120-2135.

11 Q. Wei, R. Nagi, K. Sadeghi, S. Feng, E. Yan, S. J. Ki, R. Caire, D. Tseng, and A. Ozcan, *ACS Nano*, 2014, 8, 1121-1129.

12 S. Liu, W. Chen, J. Wang, J. Wang, and F. Ma, *J. Hazard. Mater.*, 2019, **389**, 121469.

13 M. Y. Chae, J. Yoon, and A. W. Czarnik, *J. Mol. Reco.*, 1996, **9**, 297-303.

14 H. Xue, X. J. Tang, L. Z. Wu, L. P. Zhang, and C. H. Tung, *J. Org. Chem.*, 2005, **70**, 9727-9734.

15 J. Y. Lee, S. K. Kim, J. H. Jung, and J. S. Kim, *J. Org. Chem.*, 2005, **70**, 1463-1466.

16 K. Yoosaf, B. I. Ipe, C. H. Suresh, and K. G. Thomas, *J. Phys. Chem. C*, 2007, **111**, 12839-12847.

17 Y. Y. Chen, H. T. Chang, Y. C. Shiang, C. K. Chiang, and C. C. Huang, *Anal. Chem.*, 2009, **81**, 9433-9439.

18 J. J. Qin, L. X. Cao, and W. Liu, *Chin. J. Lumin.*, 2014, **35**, 858.

19 H. Wang, L. Yang, S. Chu, B. Liu, Q. Zhang, L. Zou, S. Yu, and C. Jiang, *Anal. Chem.*, 2019.

20 S. Xu, S. H. Xu, Y. S. Zhu, W. Xu, P. W. Zhou, C. Y. Zhou, B. Dong, and H. W. Song, *Nanoscale*, 2014, **6**, 12573-12579.

21 M. Li, X. Zhou, and S. Guo, *Biosens. Bioelectron.*, 2013, **43**, 69-74.

22 Q. Zhao, X. Rong, H. Ma, and G. Tao, *J. Hazard. Mater.*, 2013, **250**, 45-52.

23 J. J. Zhang, F. F. Cheng, J. J. Li, J. J. Zhu, and Y. Lu, *Nano Today*, 2016, **11**, 309-329.

24 A. N. De, C. Elosúa, J. M. Corres, and F. J. Arregui, *Sens.*, 2019, **19**, 599.

25 G. H. Jia, P. A. Tanner, C. K. Duan, and J. Dexpert-Ghys, *J. Phys. Chem. C*, 2010, **114**, 2769-2775.

26 X. J. Huang, Q. Y. Guo, S. Kang, T. C. Ouyang, Q. P Chen, X. F. Liu, Z. G. Xia, Z. M. Yang, Q. Y. Zhang, J. R. Qiu and G. P. Dong, *ACS Nano*, 2020, **14**, 3150-3158.

27 D. Q. Chen, G. Fang, and X. Chen, *ACS Appl. Mater. Interfaces*, 2017, **9**, 40477-40487.

28 C. Y. Wang, H. Lin, X. Q. Xiang, Y. Cheng, Q. M. Huang, Y. Gao, X. S. Cui, and Y. S. Wang, *J. Mater. Chem. C*, 2018, **6**, 9964-9971.

29 X. Q. Xiang, H. Lin, J. Xu, Y. Cheng, C. Y. Wang, L. Q. Zhang, and Y. S. Wang, *Chem. Eng. J.*, 2019, **378**, 122255.

30 X. J. Huang, Q. Y. Guo, D. Yang , X. D. Xiao, X. F. Liu, Z. G. Xia, F. J. Fan, J. R. Qiu and G. P. Dong, *Nat. Photonics*, 2020, **14**, 82-88.

31 Y. Wei, Z. Cheng, and J. Lin, *Chem. Soc. Rev.*, 2019, **48**, 310-350.

32 X. Q. Xiang, H. Lin, R. F. Li, Y. Cheng, Q. M. Huang, J. Xu, C. Y. Wang, X. Y. Chen, and Y. S. Wang, *Nano. Res.*, 2019, **12**, 1049-1054.

33 E.I. Kamitsos, and G.D. Chryssikos, *J. Mol. Struct.*, 1991, **247**, 1-16.

34 B. N. Meera, and J. Ramakrishna, *J. Non-Cryst. Solids*, 1993, **159**, 1-21.

35 B. N. Meera, A. K. Sood, and N. Chandrabhas, *J. Non-Cryst. Solids*, 1990, **126**, 224-230.

36 E. I. Kamitsos, M. A. Karakassides, and G. D. Chryssikos, *Phys. Chem. Glasses*, 1989, **30**, 229-234.

37 G. D. Chryssikos, E. I. Kamitsos, A. P. Patsis, and M. A. Karakassides, *Mater. Sci. Eng. B*, 1990, **7**, 1-4.

38 L. Zhang, D. Wang, Z. Hao, X. Zhang, G. H. Pan, H. Wu, and J. Zhang, *Adv. Opt. Mater.*, 2019, **7**, 1900185.

39 L. L. Zhang, J. H. Zhang, Z. D. Hao, and X. P. Yan, *Chin. J. Lumin.*, 2019, **40**, 1449-1459

40 J. F. Ramalho, S. F. Correia, and L. Fu, *Adv. Sci.*, 2019, **6**, 1900950.

41 J. C. Zhang, C. Pan, Y. F. Zhu, H. W. He, X. Liu, and J. Qiu, *Adv. Mater.*, 2018, **30**, 1804644.

A Solid-State Colorimetric Fluorescent Pb^{2+}-Sensing Scheme: Mechanically-Driven $CsPbBr_3$ Nanocrystallization in Glass

Liqiang Zhang,[a] Hang Lin,[,a] Congyong Wang,[a] Wei-Ren Liu,[b] Shuxing Li,[c] Yao Cheng,[a] Ju Xu,[a] Hang Gao,[a] Kang Li,[d,e] Nigel Copner,[d,e] Xueyuan Chen,[a] Yuansheng Wang[*,a]*

[a] Key Laboratory of Optoelectronic Materials Chemistry and Physics, Key Laboratory of Design and Assembly of Functional Nanostructures, Fujian Institute of Research on the Structure of Matter, Chinese Academy of Sciences, Fuzhou, Fujian 350002, China;
[b] Department of Chemical Engineering, R&D Center for Membrane Technology, Research Center for Circular Economy, Chung Yuan Christian University, Chung Li, Taiwan;
[c] College of Materials, Xiamen University, Xiamen, Fujian 361005, China;
[d] Wireless & Optoelectronics Research & Innovation Centre, Faculty of Computing, Engineering & Science, University of South Wales, Wales, CF37 1DL, UK;
[e] Foshan Huikang Optoelectronics Ltd., Foshan 528000, China;

[*] Corresponding Authors. E-mail: lingh@fjirsm.ac.cn; yswang@fjirsm.ac.cn

E-mail: lingh@fjirsm.ac.cn; Tel/Fax: +86-591-63179423
E-mail: yswang@fjirsm.ac.cn; Tel/Fax: +86-591-63179438

Abstract:

Highly toxic Pb^{2+} poses a great threat to the health of human beings and ecosystem, urgently calling for efficient Pb^{2+} detection method. Herein, it is demonstrated a brand-new solid-state fluorescent Pb^{2+}-sensing scheme based on a kind of Pb^{2+}-responsive borate glass powder that is able to precipitate $CsPbBr_3$ nanocrystals on glass surface upon grinding with Pb^{2+} sources, following a mechanically-driven glass crystallization mechanism. Pb^{2+} sensing is achieved by using Pb^{2+} concentration dependent green emission of $CsPbBr_3$ as indicator signal and that independent red emission of Eu^{3+} as reference signal. Under UV light irradiation, the obvious emissive color variation from red to green as Pb^{2+} concentration varies enables the intuitive Pb^{2+}-sensing by naked eyes. With the aids of spectrometer and smartphone, Pb^{2+} concentration can be quantitatively determined with the detection limit as low as ~70 ppm and ~400 ppm, respectively. The semi-quantitative Pb^{2+} detection is also possible by comparing the emissive color with the calibrated color card. Hopefully, the proposed solid-state fluorescent Pb^{2+}-sensing strategy with high selectivity can be used for portable and quick Pb^{2+} analysis in daily life.

Keywords: Pb^{2+} detection, fluorescent sensing, perovskite nanocrystals, glass crystallization, Eu^{3+}

1. Introduction

Industrial activities have brought not only tremendous wealth for human being, but unfortunately the serious environmental problems, such as heavy metal ion pollution, greenhouse gas emission, plastic abuse, and so on. Among these problems, closely relating with human health, the pollution of highly toxic metal (HTM) ions, including Hg^{2+}, Pb^{2+}, Cd^{2+} and Cr^{6+}, has aroused pressing concerns globally, since these HTM ions are non-biodegradable and accumulative in the environment through contaminating soil, water and food.[1-3] Especially, Pb^{2+} greatly threatens the children by inducing irreversible neurological damage and behavioral dysfunctions.[4-5] Pb^{2+} poisoning can also cause serious diseases, *e.g.*, memory loss, anemia, muscle paralysis, neurasthenia, limb pain, and infertility.[6-7] How to detect Pb^{2+}, even at trace level, has been a matter of vital importance for environmental protection and disease prevention.

Conventionally, Pb^{2+} detection requires sophisticated instrument (*e.g.*, the inductively coupled plasma mass spectrometer, ICP-MS) and follows complex operation procedure (sample pretreatment), and therefore, can only be carried out in the lab by a specially trained person. Recently, Pb^{2+} detection based on fluorescent method gains popularity for the merits of low detection limit, fast response time, and technical simplicity.[8-9] Particularly, with the rapid development of smartphones, the fluorescent parameters (intensity and lifetime) can be readily read by the assembled charge-coupled device (CCD) camera of smartphones, bringing about new advantages of on-site real-time detection and no needs of trained personnel.[10-12]

For the fluorescent Pb^{2+}-sensing method, the basic detection principle is always the same, *i.e.*, luminescent change or colorimetric change (when excited) dependent on Pb^{2+} concentration; however, the Pb^{2+}-sensing materials can be greatly varied from organics to inorganics according to their different application directions, and the corresponding underlying Pb^{2+}-sensing mechanisms are also quite different. One typical example is the small molecule based chemosensor, where the complexation of ligand with Pb^{2+} affects

fluorescence properties by restricting the photo-induced electron transfer with fluorophore,[13] improving electron-accepting ability of some specific groups,[14] or changing the structural conformation.[15] The functionalized Au/Ag nanoparticle is the other kind of efficient Pb^{2+} sensor, and in this case, the chelation/aggregation of Au/Ag nanoparticle in the presence of Pb^{2+} mediated by the functional groups on surface results in plasmon coupling and thus visual color change.[16-17] The functionalized quantum dots (QDs), including semiconductor QDs and carbon QDs, are newly emerged Pb^{2+}-sensors with admirable spectral characteristics of broad absorption and adjustable emission,[18-19] whose Pb^{2+}-sensing properties depend on the chelating reagents bonded to QDs: the chelation of Pb^{2+} with complex could quench QDs exciton emission for the inner filter effect [19-20] or enhance it for the inhibition of adverse fluorescence resonant energy transfer.[21-22] Nevertheless, in spite of the satisfied Pb^{2+} detection effectiveness, state-of-the-art fluorescent Pb^{2+} sensors have their disadvantage respectively. For example, the organic sensor is criticized for the poor photostability and photobleaching;[23] the practical application of Au/Ag nanoparticle is hindered by ultrahigh price;[24] and some semiconductor QDs contain highly toxic Cd,[21-22] *etc*. Moreover, all these materials are prepared via liquid-phase route, generating serious concerns of using environment-unfriendly organic solvent, low production rate, and complex preparation procedure. When applying these materials to Pb^{2+}-sensing, some other technical issues arise: 1) the liquid environment is required, and so the target analyte should be dissolved, which is inconvenient for detecting solid samples; 2) the detection accuray is subjected to acidity/alkalinity of solvent; and 3) the possible interference of the other metal ions——the detection selectivity matters.

In the present work, we proposed a new solid-state Pb^{2+}-sensing strategy based on mechanically-driven glass crystallization of $CsPbBr_3$ perovskite nanocrystals (NCs) in a Pb^{2+}-responsive borate glass system. Utilizing Pb^{2+}-dependent green emission of $CsPbBr_3$ as indicator signal and Pb^{2+}-independent red emission of Eu^{3+} as reference signal, it is

demonstrated an effective colorimetric fluorescent Pb^{2+}-sensing scheme able to visually perceive Pb^{2+} by naked eyes, and quantitatively/semi-quantitatively detect Pb^{2+} by spectrometer and mobile smartphone.

2. Experimental

2.1 Synthesis of Pb^{2+}-responsive glass powder:

The Eu^{3+} doped precursor glass (PG) with stoichiometric composition (in mol%) of $50B_2O_3$-10ZnO-10CaO-$5K_2O$-$10Cs_2O$-15NaBr (abbreviated as Eu-BZCKCN glass) was fabricated via a melt-quenching route. The raw materials of H_3BO_3, ZnO, $CaCO_3$, K_2CO_3, Cs_2CO_3, NaBr, and Eu_2O_3 were weighted and mixed thoroughly in an agate mortar and melted in a Al_2O_3 crucible at 950 ℃ for 30 min under an ambient atmosphere. Then, the glass melt was super-cooled down to 150 °C by quickly pouring into a pre-heated copper mold. After holding at 150 °C for 2 h to relinquish inner stress, the bulk PG was obtained, which was further pulverized, ball-milled for 10 h, and screened by a 400-mesh sieve, into the Eu-BZCKCN glass powders.

2.2 Fluorescent Pb^{2+}-sensing:

Fluorescent Pb^{2+} detection was performed by using the Eu-BZCKCN glass powder as Pb^{2+}-sensor, following a facile solid-state route. In a typical procedure, 1 g of the said glass powder was blended with the solid analyte and then fully ground in an agate mortar for 10 min. One can also dissolve Pb^{2+} salt in water, dilute into certain concentration, and then drip a small amount of solution into Eu-BZCKCN glass powder for reaction upon grinding. Under 365 nm UV light excitation, luminescence properties of the ground samples were recorded by the professional spectroscopic measurement or analyzed by the color recognizer software loaded in smartphone after taking photographs by CCD camera. According to the pre-calibrated relationship between Pb^{2+} concentration and luminescence intensity/RGB color information, one can determine the Pb^{2+} concentration in the analyte.

2.3 Characterization:

Differential scanning calorimetry (DSC, Netzsch, STA449F3) was carried out by heating the Eu-BZCKCN glass powder in an air atmosphere (α-Al_2O_3 crucible) at a heating rate of 10 °C/min. Transmission electron microscope (TEM, JEOL, JEM-2010) observation operating at 200 kV and scanning electron microscope (SEM, JEOL, JSM-6700F) observation equipped with an energy dispersive spectrometer (EDS, Oxford INCA) were performed to characterize microstructure of the precipitated perovskite $CsPbBr_3$ NCs on glass surface. Raman spectra (HORIBA, LabRam HR) were measured to study the glass structural variation dependent on glass composition, using a 633 nm laser as the excitation source. The photoluminescence (PL) and photoluminescence excitation (PLE) spectra were measured by a spectrophotometer (Edinburgh Instruments, FS920) equipped with a 450 W xenon lamp as the excitation source and a photomultiplier tube (R943-02, Hamamatsu) as the detector. Confocal images were taken by a confocal laser scanning microscopy system (C2/Ti-E) equipped with a Plan Fluor VC 20x DIC N2 objective lens (NA 0.5) and Andor ixon3 EMCCD camera.

3. Results and discussions

3.1 Mechanically-driven glass crystallization of $CsPbBr_3$

In Figure. 1a and 1b, one can see the prepared Eu-BZCKCN bulk glass and the corresponding glass powder yield red emission under 365 nm UV light irradiation. The steady-state spectroscopic measurements demonstrate the red emission originates from the parity-forbidden 4f↔4f transitions of Eu^{3+}, as presented in Figure. 1c. The much more intensified Eu^{3+}: $^5D_0 \rightarrow {}^7F_2$ electric-dipole transition at 615 nm than the Eu^{3+}: $^5D_0 \rightarrow {}^7F_1$ magnetic-dipole one at 590 nm reveals that, Eu^{3+} ions, possibly acting as glass network modifiers, are located in a noncentrosymmetric environment.[25] In the experiment, Eu^{3+} doping concentration is optimized as 1.5 mol%, beyond which the bulk PG becomes devitrified and therefore the red emission intensity declines. Interestingly, upon grinding the BZCKCN glass powder with Pb^{2+}-source in solid or liquid state, the ground sample yields green light under 365 nm UV light irradiation (Figure. 1d), indicative of the generation of new photo-active

species. Worthy to be mentioned, in the experiment, we chose lead acetate ($(CH_3COO)_2Pb$) as a representative, while the similar phenomena were found when using the other Pb^{2+}-containing substances, such as, PbF_2, PbO, $PbBr_2$ *etc.* The spectral features in PL/PLE spectra and kinetic decay curve of the ground sample (Figure. 1e and 1f) accord well with the excitonic excitation/emission characteristics of perovskite $CsPbBr_3$.[26-29] From the confocal laser scanning microscope analysis on single one Eu-BZCKCN glass particle (Figure. 1g-1i), it is evident that both of the green and red emissions come from glass powder, and so, this is not the case of simple physical mixture of two luminescent species upon grinding; in other words, the newly generated active centers with green emission should be incorporated into glass.

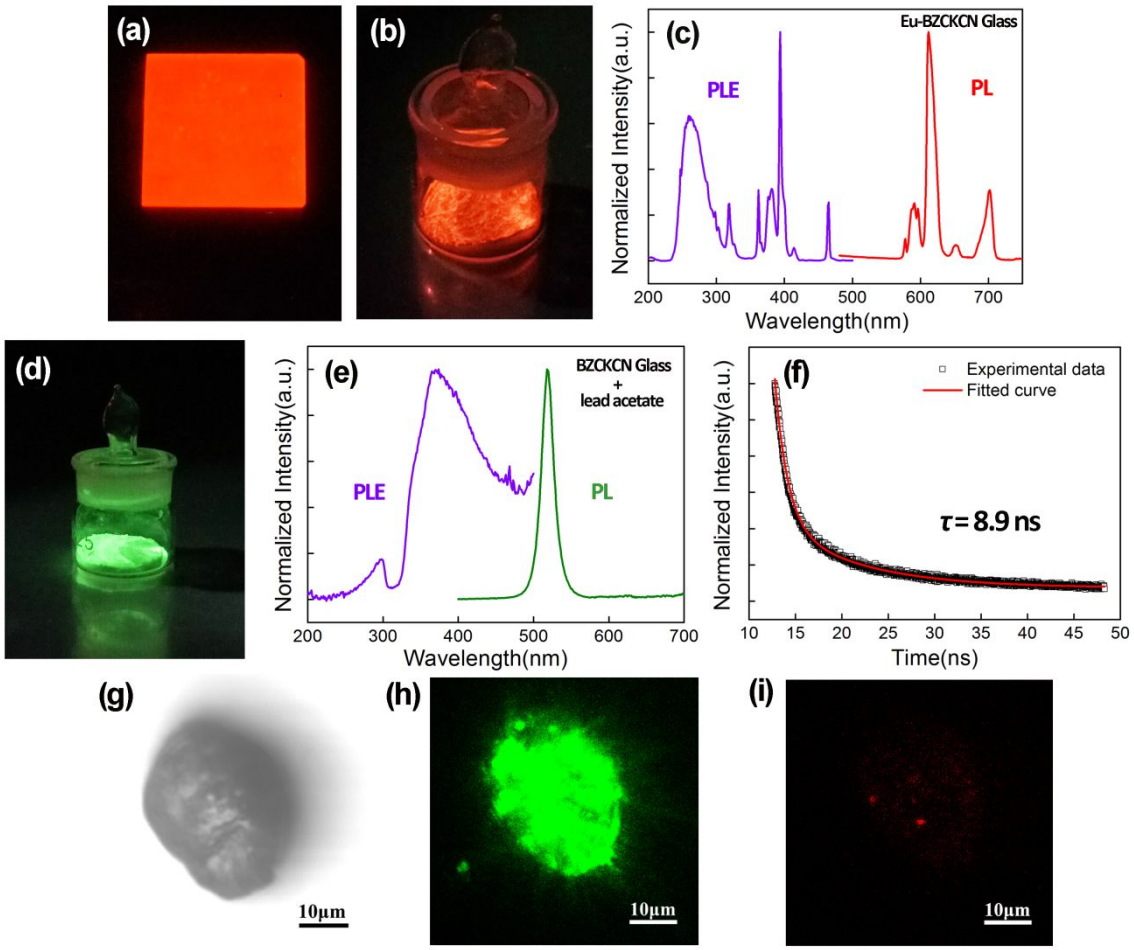

Figure. 1 Luminescent photographs of the prepared (a) Eu-BZCKCN bulk glass and (b) the corresponding glass powder, upon 365 nm UV light irradiation. (c) PL (λ_{ex}=365 nm) and PLE (λ_{em}=615 nm) spectra of the Eu-BZCKCN glass powder. (d) Luminescent photographs after grinding BZCKCN glass powder with lead

acetate, under 365 nm UV light irradiation. (e) PL (λ_{ex}=365 nm) and PLE (λ_{em}=515 nm) spectra and (f) luminescent decay curve (λ_{ex}=365 nm, λ_{em}=515 nm) of the sample after grinding Eu-BZCKCN glass powder with lead acetate. The confocal laser scanning microscope analysis on single one Eu-BZCKCN glass particle excited (g) without and (h, i) with UV laser (λ_{ex}=405 nm); for (h), the detection channel is 525 nm; for (i) the detection channel is785 nm (this is why the red emission looks so weak).

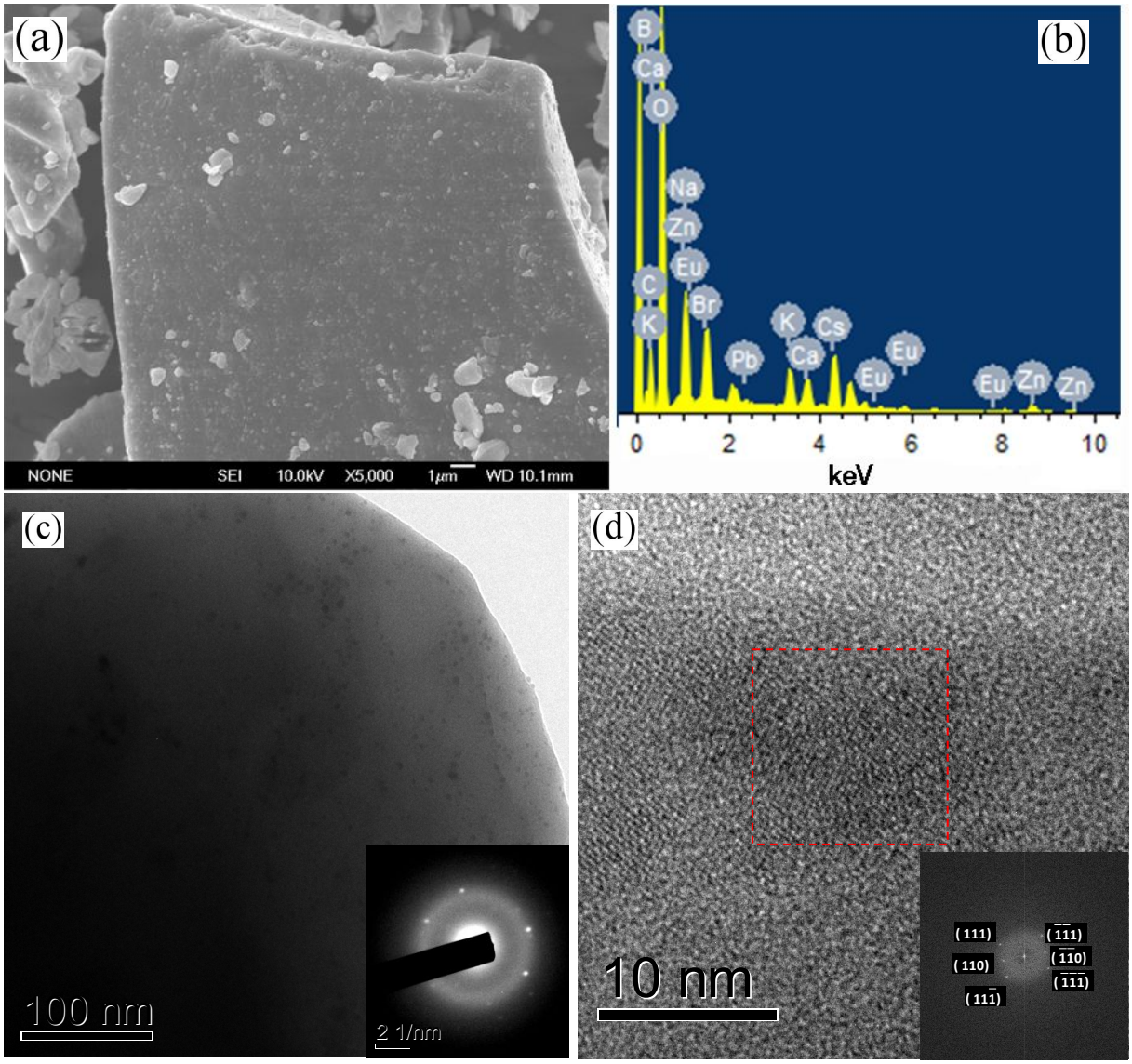

Figure. 2 (a) SEM observation on single one glass particle upon grinding Eu-BZCKCN glass powder with lead acetate, and (b) the corresponding EDS analysis result. (c) Bright-field TEM image of the sample after grinding Eu-BZCKCN glass powder with lead acetate; inset is the corresponding SAED pattern. (d) High-resolution TEM observation on single one $CsPbBr_3$ NC; inset shows the FFT pattern converted from the red dashed square region.

SEM microstructure observation discloses that some tiny particles with size up to several tens or hundreds of nanometers randomly distribute on glass surface (Figure. 2a). EDS analysis on single one glass particle confirms the glass composition of B, Zn, Ca, K, Na, Cs,

Br, O, Eu, and the post-adding Pb is also detected (Figure. 2b). We speculate that Pb^{2+} reacts with Cs^{+} and Br^{-} on glass surface to form $CsPbBr_3$, since the efficient green emitter $CsPbBr_3$ is known to crystallize easily for its ionic nature and ultralow formation energy.[28-31] In the X-ray diffraction (XRD) measurement, $CsPbBr_3$ diffraction peak cannot be discerned, which should be due to its low crystallization fraction (merely crystalizing on glass surface) beyond the detection limit (~5%) of XRD. Fortunately, the existence of $CsPbBr_3$ can be identified in the following TEM observation. The bright-field TEM image in Figure. 2c shows the crystallized $CsPbBr_3$ with size down to several nanometers (in the size range of QDs) that cannot be distinguished by SEM. It is obvious that $CsPbBr_3$ crystalizes in a wide size distribution upon grinding Eu-BZCKCN glass powder with Pb^{2+}-sources. The selected area electronic diffraction (SAED) pattern demonstrates the amorphous halo ring from glass matrix and the polycrystalline diffraction spots from $CsPbBr_3$ (inset of Figure. 2c). In the high-resolution TEM image on single one $CsPbBr_3$ NC (Figure. 2d), one can identify the interplanar spacings of 0.337 nm and 0.425 nm, indexing to (111) and (110) facets, respectively. According to the corresponding two-dimensional fast Fourier transform (FFT) image, the angle between the (111) facet and the (110) one is 36.9°, getting close with the theoretical one of 35.3°. Combining these microstructural characterization results, the precipitation of $CsPbBr_3$ NCs on glass surface is confirmed.

The crystallization of $CsPbBr_3$ NCs on Eu-BZCKCN glass surface should be driven by mechanical force. Such glass crystallization mechanism was firstly demonstrated by our group in a phosphate glass system of P_2O_5-$PbBr_2$-NaBr-Cs_2O-SrO.[32] Therein, it was found the breakage of bonding of glass network provides energy for nucleation and growth of $CsPbBr_3$ NCs, and the effect of shear stress avoids long-range migration of structural units for crystallization.[32] In the studied borate glass system of B_2O_3-ZnO-CaO-K_2O-Cs_2O-NaBr, Pb is excluded in glass composition, but is post-added. We performed some experiments to elucidate the proposed crystallization mechanism. As presented in Figure. 3a, DSC curve of

the Eu-BZCKCN glass shows glass transition temperature (T_g) of ~256 °C. Considering that the structural relaxation of glass to induce rearrangement of structural units should be at least higher than T_g, while reaching such high temperature during grinding seems impossible, the conventional heat-induced glass crystallization mechanism is believed not workable in the present case. It is also noticed that not all the Eu-BZCKCN glasses with varied glass compositions result in $CsPbBr_3$ crystallization on glass surface after grinding with Pb^{2+} source. As an example, for $50B_2O_3$-10ZnO-10CaO-$5K_2O$-(25-x)Cs_2O-xNaBr (in mol%, x = 5, 10, 15, 20), the crystallization takes place only when x>15 mol%. Therefore, it can be concluded that the mechanically-driven $CsPbBr_3$ crystallization is principally determined by the nature of glass. In Figure. 3b, we measured Raman spectra of the Eu-BZCKCN glass by varying the relative content of Cs_2O/NaBr. All the Raman peaks accord well with those vibrations of all kinds of boroxol groups.[33-36] As one can see, the structural variation of glass is rather complex. One most prominent difference in spectral feature for the samples able to precipitate $CsPbBr_3$ to those unable one is the more intensified Raman peaks at ~1250 cm^{-1} and ~1600 cm^{-1}. The peaks at 1250 cm^{-1} and ~1600 cm^{-1} are characteristic vibrations of metaborate chains[33] and metaborate rings,[37] respectively, both of which consist of three non-bridging oxygen (NBO) atoms. The other one prominent difference is the disappeared Raman peak at ~560 cm^{-1} in the samples able to precipitate $CsPbBr_3$. This ~560 cm^{-1} peak could be designated as $B\mathcal{O}_4^-$ tetrahedron ($\mathcal{O}$ represents bridging oxygen).[33] Evidently, the increase of Na and Br contents depolymerizes the glass network to induce more groups with NBO atoms, and the resultant loose glass structure enables the reaction of Cs^+ and Br^- (both acting as glass network modifiers with weak bonding) with Pb^{2+} on glass surface upon grinding. The mechanically-driven glass crystallization mechanism is schematically illustrated in Figure. 3c.

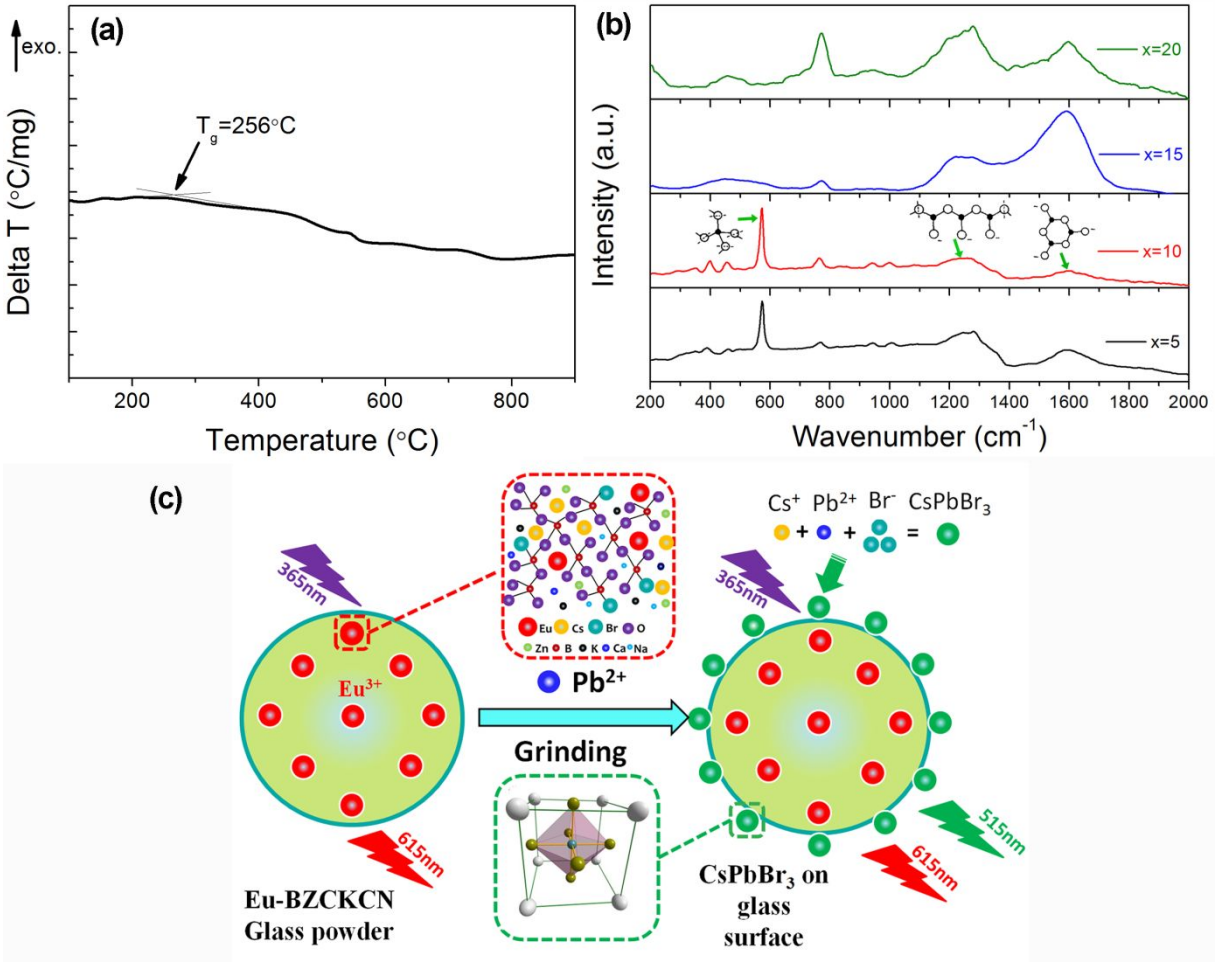

Figure. 3 (a) DSC curve of the Eu-BZCKCN glass powder. (b) Raman spectra of the Eu-BZCKCN glass with varied Cs_2O/NaBr molar ratios in $50B_2O_3$-10ZnO-10CaO-$5K_2O$-(25-x)Cs_2O-xNaBr (in mol%, x = 5, 10, 15, 20). (c) Schematic illustration of the mechanically-driven glass crystallization mechanism.

3.2 Quantitative Pb^{2+} detection via fluorescence spectrophotometer

As stated above, Eu-BZCKCN glass powder yields two-color emission after grinding with Pb^{2+} sources due to the generation of $CsPbBr_3$ NCs. We further examined Pb^{2+} concentration dependent PL spectra of the ground samples under the same instrumental setup, as displayed in Figure. 4a, wherein one can simultaneously identify the spectral features of $CsPbBr_3$ and Eu^{3+}. With the increase of Pb^{2+} concentration from 0 ppm to 3500 ppm, PL intensity of $CsPbBr_3$ gradually gets enhanced, while that of Eu^{3+} is almost unchanged; correspondingly, the PL color observed by naked eyes evolves from red to yellow, and then to green (inset of Figure. 4a). This phenomenon is reasonable: $CsPbBr_3$ NCs generate more and

more and/or they grow up accompanied with improved crystallinity, when more Pb^{2+} is supplied; while Eu^{3+} emission is obviously independent of Pb^{2+} concentration since there is no evidence of energy transfer between $CsPbBr_3$ and Eu^{3+}. The slight red-shift of excitonic emission of $CsPbBr_3$ as increasing of Pb^{2+} concentration implies the larger $CsPbBr_3$ NCs precipitate on glass surface. The more symmetric spectral profile at higher Pb^{2+} concentration suggests the particle size of $CsPbBr_3$ becomes more even. Utilizing the integrated PL intensity of $CsPbBr_3$ as indicator signal ($I_{CsPbBr3}$) and that of Eu^{3+} (I_{Eu3+}) as reference signal, a self-calibrated colorimetric Pb^{2+}-sensing scheme is demonstrated (Figure. 4b). It is found a good linearity between Pb^{2+} concentration and $I_{CsPbBr3}/I_{Eu3+}$ in the range of 0-2500 ppm, following the equation of $y=0.00105x+0.5764$ (Residual factor, $R^2=0.995$). Beyond 2500 ppm, the slope decreases, probably caused by the exhaustion of Cs^+/Br^- on glass surface. According to the equation of

$$LOD = 3\sigma / K \quad (1),$$

where LOD is the limit of detection, σ the standard deviation of blank signal, and K the slope of the fitted straight line, LOD of Pb^{2+} detection based on this solid-state fluorescent method is determined as ~70 ppm. This value is inferior to that reported in the liquid-phase fluorescent method (able to reach ppb level[24]). Despite the proposed solid-state fluorescent method is not most effective for fluorescent Pb^{2+} sensing, it is cost-effective and facile, does not bring secondary pollution to environment, and most importantly, is suitable to detect Pb^{2+} in solid form. One can expect it plays a role in detecting Pb^{2+} for solid waste, children's' toy, and so on.

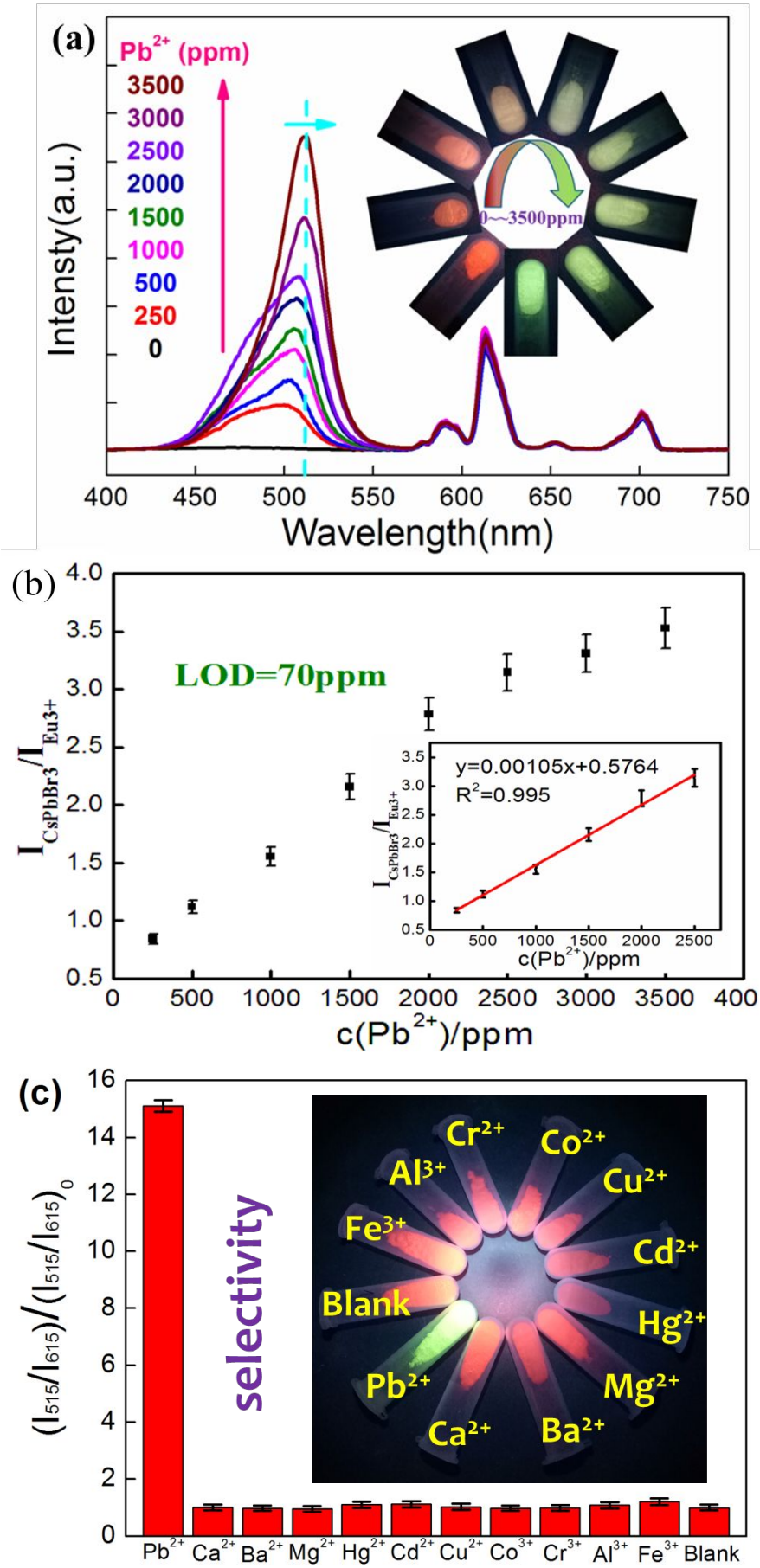
(a)
Pb2+ (ppm)
3500
3000
2500
2000
1500
1000
500
250
0
Intensty(a.u.)
0~~3500ppm
400 450 500 550 600 650 700 750
Wavelength(nm)
(b)
LOD=70ppm
y=0.00105x+0.5764
R2=0.995
ICsPbBr3/IEu3+
c(Pb2+)/ppm
(c)
(I515/I615)/(I515/I615)0
selectivity
Cr2+
Co2+
Al3+
Cu2+
Fe3+
Cd2+
Blank
Hg2+
Pb2+
Mg2+
Ca2+
Ba2+
Pb2+ Ca2+ Ba2+ Mg2+ Hg2+ Cd2+ Cu2+ Co3+ Cr3+ Al3+ Fe3+ Blank

Figure. 4 (a) Pb^{2+} concentration (0-3500 ppm) dependent PL spectra of the ground samples upon 365 nm excitation; the inset shows the corresponding luminescent photographs under 365 nm UV lamp. (b) The plot of the dependence of Pb^{2+} concentration versus $I_{CsPbBr3}/I_{Eu3+,}$ inset shows good linear relationship in the region of 0-2500 ppm. (c) The colorimetric response of other HTM ions or common cations in water/soil utilizing the proposed solid-state fluorescent method; inset shows the corresponding luminescent photographs under 365 nm UV light irradiation.

In order to evaluate the selectivity and anti-interference ability of this solid-sate fluorescent method to detect Pb^{2+}, a series of experiments were performed by grinding the Eu-BZCKCN glass powder in the presence of other HTM ions or common cations in water/soil, such as, Ca^{2+}, Ba^{2+},Mg^{2+}, Hg^{2+}, Cd^{2+}, Cu^{2+}, Co^{2+}, Cr^{3+}, Al^{3+}, and Fe^{3+}, and then measured the corresponding PL spectra of the ground samples. As presented in Figure. 4c, their PL characteristics are almost identical with the Eu-BZCKCN glass powder (as the blank sample), and so the influence of these interfering ions is negligible.

3.2 On-site real-time quantitative/semi-quantitative Pb^{2+} detection via smartphone

Nowadays, the software/hardware technologies of smartphone change with each passing day, allowing ever-closer approach between the user and the access to information. Utilizing the integrated CCD camera, the LED source, and the APP software provided by third-party Company, the spectroscopy applications of smartphones, such as, NIR light for food analysis,[38-39] smart QR codes for luminescence thermometry,[40] persistent luminescence for anti-counterfeiting,[41] as well as, fluorescent Pb^{2+}-sensing,[19] has been proposed and demonstrated recently. Herein, we will show the proposed solid-state fluorescent Pb^{2+}-sensing method is also compatible to smartphone technology for portable and quick Pb^{2+} analysis in daily life.

In Figure. 5a, we schematically illustrate the Pb^{2+}-sensing method using smartphone. The luminescent photographs of the ground samples under UV light irradiation are taken by CCD camera. Based on a simple function embedded in color recognizer software downloaded from Oppo APP Market, the color in luminescence photographs can be decomposed into three RGB channels. The obtained RGB values ($I_{green\text{-}channel}/I_{red\text{-}channel}$) correlates with Pb^{2+}

concentration (Figure. 5b). There is a good linear relationship between them in the range of 0-2500 ppm following a function of y=0.000505x+0.414 with R^2=0.986. According to equation (1), LOD of the proposed solid-state fluorescent Pb^{2+}-sensing method with the aid of smartphone is determined as ~400 ppm. A semi-quantitative detection of Pb^{2+} can also be achieved by comparing the Pb^{2+}-dependent luminescent color with the calibrated color card provided by the software.

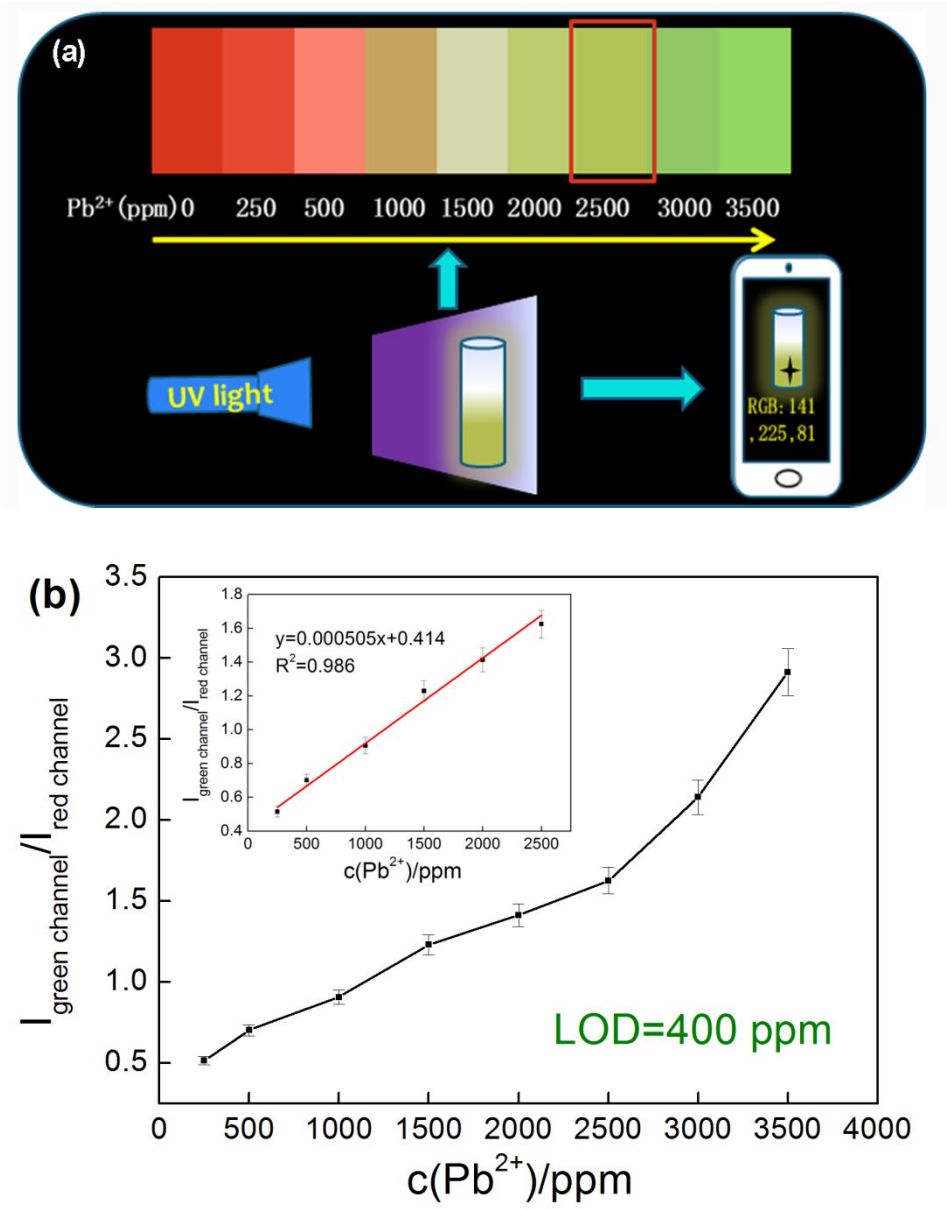

Figure. 5 (a) Schematical illustration of using smartphone to determine Pb^{2+} concentration. (b) The plot of Pb^{2+} concentration dependent color change (green channel/red channel) recognized by smartphone, inset shows good linear relationship in the region of 0-2500 ppm.

4. Conclusion

In summary, it is proposed a novel solid-state fluorescent Pb^{2+}-sensing strategy that partially settles the tough issues of high cost, inconvenience, and environment hazards, *etc.,* in the conventional liquid-phase Pb^{2+}-sensing scheme. Such Pb^{2+}-sensing strategy is achieved by grinding a Pb^{2+}-responsive Eu-BZCKCN glass powder with Pb^{2+} sources. The microstructural characterization demonstrates the precipitation of $CsPbBr_3$ NCs in a wide size distribution on glass surface. According to Raman analyses, the mechanically-driven glass crystallization behavior is closely related with the glass network structure, that is, only those loose glass network with NBO atoms enables the $CsPbBr_3$ crystallizaiton. For colorimetric Pb^{2+} detection, the Pb^{2+} concentration dependent green emission from the crystallized $CsPbBr_3$ can be used as indicator signal, while the Pb^{2+} concentration independent red emission from the doped Eu^{3+} in glass serves as reference signal. Evidently, the color variation makes the visual perception of Pb^{2+} possible. It is also verified the quantitative Pb^{2+} detection via fluorescence spectrophotometer with high selectivity and quantitative/semi-quantitative Pb^{2+} detection via smartphone for portable and quick Pb^{2+} analysis in daily life. The proposed solid-state fluorescent Pb^{2+}-sensing strategy could be realized in the other Cs- and Br- contained glass material system doped with the other active ions.

Author Contribution

H. Lin conceived the solid-state Pb^{2+} sensing scheme. L. Zhang synthesised the Pb^{2+} sensitive glass powder and wrote the first draft. H. Lin helped L. Zhang analyse the experimental results and finish the final manuscript. C. Wang and J. Xu carried out the Pb^{2+} sensing experiment. Y. Cheng helped perform the SEM/TEM measurement. W. Liu and S. Li helped to analyse the Pb^{2+} sensing mechanism. H. Gao and K. Li helped perform the spectroscopy measurements. N. Copner and X. Chen provided constructive suggestions to the data analyses. Y. Wang supervised the project.

Conflicts of interest

There are no conflicts to declare.

Acknowledgements

This work is supported by the National Natural Science Foundation of China (51972303, 11674318, 11974350, 11774346, and 51872288)

References

1 M. F. Philips, A. I. Gopalan, and K. P. Lee, *J. Hazard. Mater.*, 2012, 237, 46-54.

2 X. Qing, Z. Yutong, and G. L. Sheng, *Ecotoxicol. Environ. Saf.*, 2015, 120, 377-385.

3 N. Saha, M. S. Rahman, M. B. Ahmed, J. L. Zhou, H. H. Ngo, and W. Guo, *J. Soil Sci. Environ. Manage.*, 2017, **185**, 70-78.

4 E. S. Claudio, H. A. Goldwin, and J. S. Magyar, *Prog. Inorg. Chem.*, 2003, 51, 1-144.

5 Q. Zhu, L. Liu, Y. Xing, and X. Zhou, *J. Hazard. Mater.*, 2018, **355**, 50-55.

6 Y. Wang, and J. Irudayaraj, *Chem. Commun.*, 2011, 47, 4394-4396.

7 B. Wang, B. Luo, M. Liang, J. Wang, Y. Fang, and L. Zhi, *Nanoscale*, 2011, 3, 5059-5066.

8 T. Sokalski, A. Ceresas, T. Zwickl, and E. Pretsch, *J. Am. Chem. Soc.*, 1997, **119**, 11347-11348.

9 J. Mayer, A. Robert-Moreno, J. Sharpe, and J. Swoger, *Light: Sci. Appl.*, 2018, **7**, 70.

10 X. Chen, Y. Zhou, X. Peng, and J. Yoon, *Chem. Soc. Rev.*, 2010, 39, 2120-2135.

11 Q. Wei, R. Nagi, K. Sadeghi, S. Feng, E. Yan, S. J. Ki, R. Caire, D. Tseng, and A. Ozcan, *ACS Nano*, 2014, 8, 1121-1129.

12 S. Liu, W. Chen, J. Wang, J. Wang, and F. Ma, *J. Hazard. Mater.*, 2019, **389**, 121469.

13 M. Y. Chae, J. Yoon, and A. W. Czarnik, *J. Mol. Reco.*, 1996, **9**, 297-303.

14 H. Xue, X. J. Tang, L. Z. Wu, L. P. Zhang, and C. H. Tung, *J. Org. Chem.*, 2005, **70**, 9727-9734.

15 J. Y. Lee, S. K. Kim, J. H. Jung, and J. S. Kim, *J. Org. Chem.*, 2005, **70**, 1463-1466.

16 K. Yoosaf, B. I. Ipe, C. H. Suresh, and K. G. Thomas, *J. Phys. Chem. C*, 2007, **111**, 12839-12847.

17 Y. Y. Chen, H. T. Chang, Y. C. Shiang, C. K. Chiang, and C. C. Huang, *Anal. Chem.*, 2009, **81**, 9433-9439.

18 J. J. Qin, L. X. Cao, and W. Liu, *Chin. J. Lumin.*, 2014, **35**, 858.

19 H. Wang, L. Yang, S. Chu, B. Liu, Q. Zhang, L. Zou, S. Yu, and C. Jiang, *Anal. Chem.*, 2019.

20 S. Xu, S. H. Xu, Y. S. Zhu, W. Xu, P. W. Zhou, C. Y. Zhou, B. Dong, and H. W. Song, *Nanoscale*, 2014, **6**, 12573-12579.

21 M. Li, X. Zhou, and S. Guo, *Biosens. Bioelectron.*, 2013, **43**, 69-74.

22 Q. Zhao, X. Rong, H. Ma, and G. Tao, *J. Hazard. Mater.*, 2013, **250**, 45-52.

23 J. J. Zhang, F. F. Cheng, J. J. Li, J. J. Zhu, and Y. Lu, *Nano Today*, 2016, **11**, 309-329.

24 A. N. De, C. Elosúa, J. M. Corres, and F. J. Arregui, *Sens.*, 2019, **19**, 599.

25 G. H. Jia, P. A. Tanner, C. K. Duan, and J. Dexpert-Ghys, *J. Phys. Chem. C*, 2010, **114**, 2769-2775.

26 X. J. Huang, Q. Y. Guo, S. Kang, T. C. Ouyang, Q. P Chen, X. F. Liu, Z. G. Xia, Z. M. Yang, Q. Y. Zhang, J. R. Qiu and G. P. Dong, *ACS Nano*, 2020, **14**, 3150-3158.

27 D. Q. Chen, G. Fang, and X. Chen, *ACS Appl. Mater. Interfaces*, 2017, **9**, 40477-40487.

28 C. Y. Wang, H. Lin, X. Q. Xiang, Y. Cheng, Q. M. Huang, Y. Gao, X. S. Cui, and Y. S. Wang, *J. Mater. Chem. C*, 2018, **6**, 9964-9971.

29 X. Q. Xiang, H. Lin, J. Xu, Y. Cheng, C. Y. Wang, L. Q. Zhang, and Y. S. Wang, *Chem. Eng. J.*, 2019, **378**, 122255.

30 X. J. Huang, Q. Y. Guo, D. Yang , X. D. Xiao, X. F. Liu, Z. G. Xia, F. J. Fan, J. R. Qiu and G. P. Dong, *Nat. Photonics*, 2020, **14**, 82-88.

31 Y. Wei, Z. Cheng, and J. Lin, *Chem. Soc. Rev.*, 2019, **48**, 310-350.

32 X. Q. Xiang, H. Lin, R. F. Li, Y. Cheng, Q. M. Huang, J. Xu, C. Y. Wang, X. Y. Chen, and Y. S. Wang, *Nano. Res.*, 2019, **12**, 1049-1054.

33 E.I. Kamitsos, and G.D. Chryssikos, *J. Mol. Struct.*, 1991, **247**, 1-16.

34 B. N. Meera, and J. Ramakrishna, *J. Non-Cryst. Solids*, 1993, **159**, 1-21.

35 B. N. Meera, A. K. Sood, and N. Chandrabhas, *J. Non-Cryst. Solids*, 1990, **126**, 224-230.

36 E. I. Kamitsos, M. A. Karakassides, and G. D. Chryssikos, *Phys. Chem. Glasses*, 1989, **30**, 229-234.

37 G. D. Chryssikos, E. I. Kamitsos, A. P. Patsis, and M. A. Karakassides, *Mater. Sci. Eng. B*, 1990, **7**, 1-4.

38 L. Zhang, D. Wang, Z. Hao, X. Zhang, G. H. Pan, H. Wu, and J. Zhang, *Adv. Opt. Mater.*, 2019, **7**, 1900185.

39 L. L. Zhang, J. H. Zhang, Z. D. Hao, and X. P. Yan, *Chin. J. Lumin.*, 2019, **40**, 1449-1459

40 J. F. Ramalho, S. F. Correia, and L. Fu, *Adv. Sci.*, 2019, **6**, 1900950.

41 J. C. Zhang, C. Pan, Y. F. Zhu, H. W. He, X. Liu, and J. Qiu, *Adv. Mater.*, 2018, **30**, 1804644.

Table of Contents

Herein, it is proposed a brand-new solid-state Pb^{2+}-sensing strategy based on mechanically-driven glass crystallization in a Pb^{2+}-responsive borate glass system.